Quasiparton distribution functions in covariant quark models

F. Aslan,[1,3] A. Tandogan,[2] and P. Schweitzer[3]
[1]*Department of Physics, Chemistry and Mathematics, Alabama A&M University, Normal, Alabama 35762, USA*
[2]*Department of Physics, University of Connecticut, Hartford, Connecticut 06103, USA*
[3]*Department of Physics, University of Connecticut, Storrs, Connecticut 06269-3046, USA*

(Received 31 May 2026; accepted 23 September 2026; published 30 October 2026)

Quasiparton distribution functions (QPDFs) are defined in terms of QCD fields at spacelike separations evaluated in matrix elements of hadrons moving with velocity v. These objects can be studied in lattice QCD. In the limit when v approaches the speed of light, QPDFs converge to parton distribution functions. It is insightful to study QPDFs and their convergence in models. In this work, we first study the QPDFs in a broad class of quark models characterized by one common feature, namely the absence of gauge degrees of freedom. We provide general proofs for the convergence and sum rules of the unpolarized quark and antiquark QPDFs for both choices γ^0 and γ^3. We choose the covariant parton model as an illustration, and derive analytical results for the small-x_v behavior of QPDFs and the energy-momentum tensor form factor $\bar{c}^q(t)$ at zero momentum transfer. These results are of interest as they correspond to a Wandzura-Wilczek-type approximation.

DOI: 10.1103/bl2f-xygk

I. INTRODUCTION

Parton distribution functions (PDFs) [1] play an important role in the description of the internal structure of hadrons in factorizable deep-inelastic scattering processes [2]. PDFs are frame-independent functions defined in terms of nonlocal QCD field operators with lightlike separations, for instance, in the twist-2 unpolarized quark case one deals with operators of the type $\bar{\Psi}^q(0)\mathcal{W}(0,z)\gamma^+\Psi^q(z)$ with $z^2=0$, where $\mathcal{W}$ denotes the Wilson line and $\gamma^+=(\gamma^0+\gamma^3)/\sqrt{2}$. It was not known how to compute the x-dependence of PDFs in Euclidean space-time in lattice QCD until the concept of quasi-PDFs (QPDFs) was introduced [3]. QPDFs are frame dependent and defined in terms of nonlocal QCD operators with spacelike separations, for instance, in the quark case $\bar{\Psi}^q(0)\mathcal{W}(0,z)\Gamma\Psi^q(z)$ with $z^2<0$ where $\Gamma=\gamma^0$ or γ^3 can be chosen, which are evaluated in matrix elements of hadrons moving with a velocity v. In the limit when v approaches the speed of light, one recovers from QPDFs the frame-independent PDFs [3,4]. Noteworthy is a prior discussion of the QPDF concept in a model application [5].

The two operations, (i) taking the limit $v\to 1$ (we use natural units with $c=\hbar=1$) and (ii) carrying out the renormalization of operators, do not commute, which introduces important differences between PDFs and QPDFs. For instance, the latter contain higher-twist corrections suppressed by powers of $P_z=Mv/\sqrt{1-v^2}$ and have different renormalization properties which are determined systematically order by order in perturbative QCD matching calculations; see, e.g., [6–9]. Lattice QCD calculations of QPDFs were reported in, e.g., Refs. [10–29]. For other methods to study partonic properties of hadrons on Euclidean lattices see Refs. [30–40] and the reviews [41–46].

In this work we will present a study of QPDFs in quark models. Model studies of QPDFs have been carried out in a variety of frameworks and are of interest for their own sake [47–61]. While lattice QCD is a reliable first-principle nonperturbative approach to hadron structure studies, it also comes with nontrivial limitations. For instance, when taking the limit of QPDFs for $v\to 1$ or equivalently $P_z\to\infty$, power corrections appear which are generically of the type $M^2/(x_v^2(1-x_v)P_z^2)$ [41–46]. The power corrections limit the applicability of lattice calculations to the region of intermediate x_v. In models, some of the power corrections might be absent or exactly calculable owing to the simpler model dynamics and depending on the model approach. This may allow one, for instance, to draw conclusions about how QPDFs converge toward PDFs when the limit $v\to 1$ is taken or make other interesting observations. If a model shares some features of QCD, such observations can be helpful, e.g., to better understand lattice studies.

Published by the American Physical Society under the terms of the Creative Commons Attribution 4.0 International license. Further distribution of this work must maintain attribution to the author(s) and the published article's title, journal citation, and DOI. Funded by SCOAP³.

This work consists of two parts. The first part is devoted to a general discussion of QPDFs in quark models, i.e., approaches with quark and antiquark but without gauge field degrees of freedom. In this part, we define the unpolarized QPDFs in quark models in terms of the Lorentz-invariant amplitudes A_i^q and $A_i^{\bar{q}}$ which characterize the Lorentz structure of quark and antiquark correlators and are functions of $P\cdot k$ and k^2, where P^μ and k^μ denote, respectively, the nucleon and quark momenta. We show how QPDFs converge to PDFs, and give independent derivations of sum rules for QPDFs. We also discuss the interesting connection between QPDFs and transverse momentum dependent PDFs (TMDs). We will see that it is convenient to formulate QPDFs as functions of hadron velocity v rather than hadron momentum P_z, although both formulations are of course equivalent. This part applies to any quark model framework which satisfies two very general conditions, namely (i) Lorentz symmetry, and (ii) the amplitudes $A_i^q(P\cdot k, k^2)$ are either finite or, if the model exhibits any type of divergences, are renormalized or regularized such that Lorentz invariance is preserved.

In the second part, we choose for definiteness a specific model for hadron structure, namely the covariant parton model (CPM). This model is a systematic extension of Feynman's parton model concept [62,63] to the description of the partonic structure of hadrons and has been applied with success to the description of structure functions, PDFs, and TMDs [64–79]. A similar approach was pursued in [80]. Distinguished by its clarity, this model offers a convenient theoretical laboratory to investigate in a lucid way the properties of QPDFs. We derive the CPM results for QPDFs for quarks and antiquarks, demonstrate their convergence, prove their sum rules, and derive their small- and large-x_v properties which can be studied analytically in that model. We show numerical results for the QPDFs for the flavors u, d, $\bar{u}$, $\bar{d}$, s, $\bar{s}$ in the CPM and compare their convergence for the cases $\Gamma=\gamma^0$ and γ^3 in detail. The CPM results refer to a high renormalization scale μ^2 where the partonic picture is justified. Remarkably, the CPM results practically constitute a Wandzura-Wilczek approximation for the QPDFs and automatically entail the complete target-mass corrections. The Appendixes contain derivations of the CPM expressions for the electromagnetic and energy-momentum tensor form factors at $t=0$ required for the sum rules.

II. QPDFS IN GENERAL QUARK MODELS

In this section, we discuss the definition and representation of QPDFs and the proofs of their properties in general quark model frameworks defined as effective approaches without explicit gauge field degrees of freedom. The only underlying assumptions are (i) that the models respect Lorentz symmetry, and (ii) that, if divergences occur, then they are assumed to be regularized or renormalized such that relativistic invariance of the model is manifestly preserved. It is understood that the model results refer to a scale fixed in a specific way in a given model which corresponds to the renormalization scale in QCD. The scale dependence will not be indicated explicitly in the following.

A. Notation and choice of variables

In this work, we will denote the unpolarized QPDF as $D^a(x_v,\Gamma,v)$ with the two choices $\Gamma=\gamma^0$ or γ^3. In the limit when the nucleon velocity $v\to 1$, both choices converge to the unpolarized PDF $f_1^a(x)$. Some comments are in order.

First, it is important to distinguish the Lorentz-invariant variable x of PDFs from the frame-dependent variable x_v of QPDFs, where the index v stands for the nucleon velocity and indicates the frame dependence. If P^μ denotes the nucleon four-momentum and k^μ the parton four-momentum, then x and x_v are, respectively, defined as

$$x_v=\frac{k^3}{P^3},\qquad x=\frac{k^+}{P^+} \tag{1}$$

with the light cone coordinates $k^\pm=(k^0\pm k^3)/\sqrt{2}$ and $\vec{k}_\perp=(k^1,k^2)$. The light cone is selected by the hard momentum flow in a process, e.g., the virtual photon momentum in deep-inelastic electron-nucleon scattering. We will use the notations $k^\mu=(k^0,k^1,k^2,k^3)=(k^0,\vec{k}_\perp,k^3)=(k^+,\vec{k}_\perp,k^-)$ interchangeably depending on what is more convenient. Notice that k^μ is a dummy integration variable which will be introduced below in Sec. II C when expressing PDFs and QPDFs in terms of the quark correlator, i.e., no reference to the parton model is required when speaking of the "parton four-momentum" k^μ. By definition, the nucleon momentum P^μ has no transverse components.

Second, the variable x is Lorentz invariant in the sense of being boost invariant along the light cone, i.e., we obtain the same, frame-independent PDF independently of whether the nucleon is at rest, moves with a velocity $0<v<1$, or is boosted to the infinite-momentum frame $v\to 1$. The situation is different for the manifestly frame-dependent variable x_v which can be related to x as follows (see remark below):

$$x_v=\frac{x}{v}-\frac{(1-v)}{v}\frac{P\cdot k}{M^2}, \tag{2}$$

where M is the nucleon mass. The variable $P\cdot k$ appears naturally in the momentum-space description of the quark correlator and is of course a Lorentz scalar. Equation (2) shows that x_v is velocity dependent and becomes equal to x only for $v\to 1$. We remark that Eq. (2) is not a "stand-alone relation" but is valid only under the integration over d^4k with the understanding that $x_v=k^3/P^3$ and $x=k^+/P^+$

are "abbreviations." The literal meaning of x_v or x (but not both at the same time) exists only in the definitions of QPDFs and PDFs where the quark correlator is integrated over d^4k in conjunction with the appropriate δ-functions $\delta(x_v - k^3/P^3)$ or $\delta(x - k^+/P^+)$, respectively.

Third, in QCD studies $P_z = P^3 = Mv/\sqrt{1-v^2}$ is customarily used as argument for QPDFs instead of v. The two variables are equivalent, but for our purposes v is more convenient for two reasons. (i) The model expressions are more concise and elegant with v. (ii) Since $v = P_z/P_0$ with $P_0 = \sqrt{M^2 + P_z^2}$, the variable v corresponds effectively to the resummation of an infinite series in powers of M^2/P_z^2 (assuming $P_z > M$) which is evident from $v = \frac{1}{\sqrt{1+M^2/P_z^2}}$.

B. Definition and general properties

In quark models, the unpolarized PDF and QPDF are defined as

$$f_1^q(x) = \int \frac{dz^-}{4\pi} e^{-ixP^+z^-} \langle N_v|\bar{\Psi}_q(0)\gamma^+\Psi_q(z)|N_v\rangle\Big|_{z^+=0,\vec{z}_\perp=0}, \tag{3}$$

$$D^q(x_v,\Gamma,v) = \int \frac{dz^3}{4\pi} e^{-ix_vP^3z^3} \times \langle N_v|\bar{\Psi}_q(0)\Gamma\Psi_q(z)|N_v\rangle\Big|_{z^\mu=(0,0,0,z^3)}, \tag{4}$$

where $|N_v\rangle$ denotes the state of a nucleon moving with the velocity v and momentum $P^\mu = M(1,0,0,v)/\sqrt{1-v^2}$ along the z-axis. We will often use the notation $P^\mu = (P^0,0,0,P^3) = (P_0,0,0,P_z)$. The definitions of the corresponding antiquark distributions follow from the relations

$$f_1^{\bar{q}}(x) = -f_1^q(-x),$$
$$D^{\bar{q}}(x_v,\Gamma,v) = -D^q(-x_v,\Gamma,v). \tag{5}$$

PDFs are nonzero only in the region $-1 < x < 1$, while the QPDFs extend over the whole region $-\infty < x_v < \infty$.

The PDF in Eq. (3) is invariant under boosts along the z-axis, i.e., independent of the nucleon velocity v. This allows one to evaluate PDFs in any frame including the nucleon rest frame, but at the price of lightlike separated quark fields, which hinders an evaluation in Euclidean space-time in lattice QCD. In contrast to this, in the QPDF in Eq. (4), the separation of the quark fields is spacelike, which makes a computation on a Euclidean lattice possible, but the QPDF is frame dependent, and the connection to a PDF requires the limit $v \to 1$.

Except for the Wilson line absent in quark models, Eq. (4) corresponds to the QCD definition of Ref. [3] where QPDFs were introduced with applications to lattice QCD in mind. QPDFs were introduced prior to that in Ref. [5] for a different purpose, namely to prove that, in the chiral quark-soliton model, the PDFs obtained from evaluating the (i) operator definition in Eq. (3) are equivalent to (ii) probabilistic parton densities in infinite-momentum frame. To the best of our knowledge, this is the only model where this was explicitly proven [5].

The QPDFs have the following important properties. In the limit of the nucleon velocity v approaching the speed of light, the QPDFs and PDFs are connected as follows:

$$\lim_{v\to1} x_v = x, \quad \lim_{v\to1} D^q(x_v,\Gamma,v) = f_1^q(x), \quad \Gamma = \gamma^0,\gamma^3. \tag{6}$$

Other important properties are the sum rules for the first and second Mellin moments [55]. For PDFs we have

$$\int_{-1}^{1} dx\, f_1^q(x) = N^q, \tag{7}$$

$$\int_{-1}^{1} dx x\, f_1^q(x) = A^q(0), \tag{8}$$

where N^q denotes the number of valence quarks of flavor q, and $A^q(t)$ is a form factor of the energy-momentum tensor with the property that summation over all quark flavors and gluons yields $\sum_a A^a(0) = 1$ [81,82]. For the QPDFs, the corresponding sum rules in the case $\Gamma = \gamma^0$ are given by

$$\int_{-\infty}^{\infty} dx_v\, D^q(x_v,\gamma^0,v) = \frac{N^q}{v}, \tag{9}$$

$$\int_{-\infty}^{\infty} dx_v x_v\, D^q(x_v,\gamma^0,v) = \frac{A^q(0)}{v}, \tag{10}$$

while in the case $\Gamma = \gamma^3$ they are given by

$$\int_{-\infty}^{\infty} dx_v\, D^q(x_v,\gamma^3,v) = N^q, \tag{11}$$

$$\int_{-\infty}^{\infty} dx_v\, x_v\, D^q(x_v,\gamma^3,v) = A^q(0) - \frac{1-v^2}{v^2}\bar{c}^q(0), \tag{12}$$

where $\bar{c}^a(t)$ is the form factor expressing the nonconservation of the individual quark and gluon contributions to the energy-momentum tensor which vanishes upon the summation over all constituents $\sum_a \bar{c}^a(t) = 0$ [81,82].

In Refs. [34,35] a relation between one of the QPDFs and the TMD $f_1^q(x,\vec{k}_T^2)$ was derived which, in our convention, is given by the formula (see Appendix A for conventions)

$$D^q(x_v,\gamma^0,v) = P_0 \int_{-1}^{1} dx \int_{-\infty}^{\infty} dk_1\, f_1^q(x, k_1^2 + (x_v - x)^2 P_z^2). \tag{13}$$

The TMD entering this formula is defined in QCD with a straight gauge link and constitutes a field-theoretical object

which can be computed in lattice QCD but differs from what is measured in deep-inelastic scattering reactions. In quark models where gauge links are not present, the "usual" TMD enters Eq. (13).

C. Expressions in terms of Lorentz-invariant amplitudes $A_i^q(P\cdot k, k^2)$

For our purposes, it will be convenient to rewrite the definitions in Eqs. (3), (4) in terms of the unintegrated quark correlator, which is defined in quark models as follows [83]:

$$\Phi_{ij}^q(k,P,S) = \int \frac{\mathrm{d}^4 z}{(2\pi)^4} \mathrm{e}^{ik\cdot z} \langle N_v|\bar{\Psi}_j^q(0)\Psi_i^q(z)|N_v\rangle. \tag{14}$$

There is an analog definition for the antiquark correlator which is related to the quark correlator by the field-theoretic relation $\Phi_{ij}^{\bar{q}}(k,P,S) = -\Phi_{ij}^q(-k,P,S)$ [83]. In quark models the correlator is a function of the quark momentum k^μ, the nucleon momentum P^μ, and nucleon polarization vector S^μ. In QCD the correlator definitions include Wilson lines. As a consequence, the correlators in QCD depend on an additional four-vector n^μ which specifies a direction along which the Wilson lines are chosen according to the factorization theorem of a specific process [84]. By making use of the correlator in Eq. (14), the PDF and QPDF in Eqs. (3), (4) are given by

$$f_1^q(x) = \frac{1}{2P^+}\int d^4k\, \mathrm{tr}[\Phi^q(k,P,S)\gamma^+]\delta\left(x-\frac{k^+}{P^+}\right), \tag{15}$$

$$D^q(x_v,\Gamma,v) = \frac{1}{2P^3}\int d^4k\, \mathrm{tr}[\Phi^q(k,P,S)\Gamma]\delta\left(x_v-\frac{k^3}{P^3}\right). \tag{16}$$

In QCD the fully unintegrated quark correlator with a general gauge-link geometry can be decomposed into 32 linearly independent Lorentz structures constructed from the four-vectors k^μ, P^μ, S^μ, and n^μ, where n^μ specifies an independent gauge-link direction [84]. In quark models without explicit gauge-field degrees of freedom, the Wilson-line-dependent structures are absent, and the correlator is described by only 12 independent amplitudes, $A_i^q = A_i^q(P\cdot k, k^2)$, which are functions of the Lorentz scalars $P\cdot k$ and k^2 (which we often do not indicate explicitly for notational simplicity) [83]. The reduced number of linearly independent Lorentz structures in quark models implies quark-model relations among leading- and subleading-twist transverse-momentum-dependent PDFs; see, for example, Refs. [85,86]. The decomposition of the quark correlator in quark models (analog for the antiquark correlator) is as follows [87]:

$$\begin{aligned}\Phi^a(k,P,S) = {} & MA_1^a + \not{P}A_2^a + \not{k}A_3^a + \frac{i}{2M}[\not{P},\not{k}]A_4^a \\ & + i(k\cdot S)\gamma_5 A_5^a + M\not{S}\gamma_5 A_6^a + \frac{(k\cdot S)}{M}\not{P}\gamma_5 A_7^a \\ & + \frac{(k\cdot S)}{M}\not{k}\gamma_5 A_8^a + \frac{[\not{P},\not{S}]}{2}\gamma_5 A_9^a + \frac{[\not{k},\not{S}]}{2}\gamma_5 A_{10}^a \\ & + \frac{(k\cdot S)}{2M^2}[\not{P},\not{k}]\gamma_5 A_{11}^a + \frac{1}{M}\epsilon^{\mu\nu\rho\sigma}\gamma_\mu P_\nu k_\rho S_\sigma A_{12}^a.\end{aligned} \tag{17}$$

Equation (17) applies generally to *all* quark models without explicit gauge-field degrees of freedom. Note that in QCD and models with gluons, besides the 12 $A_i^q(P\cdot k, k^2)$ amplitudes in Eq. (17), 20 additional $B_i^q(P\cdot k, k^2)$ amplitudes appear due to the vector n^μ [84].

In our case, we are interested in the projection of the correlator on the Dirac structure γ^μ which yields

$$\mathrm{tr}[\Phi^q(k,P,S)\gamma^\mu] = 4(P^\mu A_2^q + k^\mu A_3^q). \tag{18}$$

In this way, the expressions for the unpolarized PDF and QPDF are given by

$$f_1^q(x) = 2\int d^4k (A_2^q + xA_3^q)\delta\left(x-\frac{k^+}{P^+}\right), \tag{19}$$

$$\begin{aligned}D^q(x_v,\gamma^\mu,v) = {} & 2\int d^4k\left(\frac{P^\mu}{P^3}A_2^q + \frac{k^\mu}{P^3}A_3^q\right)\delta\left(x_v-\frac{k^3}{P^3}\right), \\ & \mu = 0,3.\end{aligned} \tag{20}$$

The corresponding expressions for antiquarks follow from Eq. (5) by exploring $\Phi_{ij}^{\bar{q}}(k,P,S) = -\Phi_{ij}^q(-k,P,S)$ [83] which implies for the amplitudes $A_2^q(-P\cdot k, k^2) = -A_2^{\bar{q}}(P\cdot k, k^2)$ and $A_3^q(-P\cdot k, k^2) = A_3^{\bar{q}}(P\cdot k, k^2)$ [78].

D. Infinite momentum frame limit

In this section we show that the quark model expressions for QPDFs (20) yield the PDF (19) in the limit $v\to 1$. The amplitudes A_i^q, their arguments $P\cdot k$ and k^2, and d^4k are Lorentz scalars which can be evaluated in any frame. But for the specific components of P^μ and k^μ, we must choose a specific frame. It is convenient to choose a frame in which the nucleon and quark momenta are the results of a boost from the nucleon rest frame, where we have

$$P^\mu = (M,0,0,0), \quad k^\mu = (k^0,k^1,k^2,k^3)\ \text{(restframe)}, \tag{21}$$

to a frame where the nucleon moves with velocity v. The nucleon and quark four-momenta in this frame are given by

$$P^\mu = \left(\frac{M}{\sqrt{1-v^2}}, 0, 0, \frac{Mv}{\sqrt{1-v^2}}\right),$$
$$k^\mu = \left(\frac{k^0 + vk^3}{\sqrt{1-v^2}}, k^1, k^2, \frac{k^3 + vk^0}{\sqrt{1-v^2}}\right)$$
(boost from rest frame). (22)

The evaluation of the model expressions is facilitated by the fact that the amplitudes A_i^q as well as $P\cdot k$, k^2, and d^4k are Lorentz scalars, which means that the integrations can be carried out in any frame. We will make use of this property. For instance, evaluating $P\cdot k$ in the frame (22) yields $P\cdot k = Mk^0$, which is equivalent to evaluating this scalar product in the rest frame (21), although the nucleon of course moves with the velocity v. This illustrates that (i) $P\cdot k$ can of course be evaluated in any frame including the nucleon rest frame; (ii) as a Lorentz scalar it must be velocity independent, as is the case. In the frame (22) the arguments of amplitudes are given by $A_i^q = A_i^q(Mk^0, k^2)$, which has a practical advantage: in this frame the amplitudes are rotationally symmetric and even functions of the 3-momentum components k^i. Despite choosing a preferred reference frame for the d^4k-integration, the PDF expressions are nevertheless frame independent, and those for QPDFs have the correct frame (velocity) dependence.

From Eq. (22) we see that $k^+/P^+ = (k^0 + k^3)/M$ is velocity independent, and hence, so is the PDF, which is expected. By exploring the δ-function in Eq. (19) to replace x by $k^+/P^+ = (k^0 + k^3)/M$ we obtain for the PDF

$$f_1^q(x) = 2\int d^4k \left(A_2^q + \frac{k^0 + k^3}{M} A_3^q\right)\delta\left(x - \frac{k^0 + k^3}{M}\right), \quad (23)$$

which will be a helpful reference expression in the following. For the QPDFs with $\Gamma = \gamma^0, \gamma^3$ we obtain

$$D^q(x_v, \gamma^0, v) = 2\int d^4k \left(\frac{A_2^q}{v} + \frac{k^0 + vk^3}{vM} A_3^q\right) \times \delta\left(x_v - \frac{k^3 + vk^0}{vM}\right), \quad (24)$$

$$D^q(x_v, \gamma^3, v) = 2\int d^4k \left(A_2^q + \frac{k^3 + vk^0}{vM} A_3^q\right) \times \delta\left(x_v - \frac{k^3 + vk^0}{vM}\right). \quad (25)$$

In both expressions it is straightforward to take the limit $v \to 1$, and we recover in both cases the PDF in Eq. (23).

E. Flavor number sum rule

In this section, we show how the flavor number sum rule is satisfied in quark models. Let us first derive the sum rule for the PDF. In our reference frame (22) in the representation of Eq. (23) we obtain

$$\int dx\, f_1^q(x) = 2\int d^4k \left(A_2^q + \frac{k^0}{M} A_3^q\right), \quad (26)$$

where a term proportional to $k^3 A_3^q$ dropped out due to rotational symmetry of the integrand, which emerges after x-integration when the z-axis is no longer singled out. Alternatively, after x-integration one may substitute under the d^4k integral $k^3 \to (-k^3)$ to see that this term changes sign and drops out. Keep in mind that in the frame (22) we have $A_i^q = A_i^q(Mk^0, k^2)$, which are even functions of spatial components k^i and invariant under rotations. The result can be formulated also in a covariant way; see Appendix B, where we will also show how the expression on the right-hand side of Eq. (26) is related to the flavor quantum number N^q in Eq. (26).

We now derive the flavor sum rule for the case $\Gamma = \gamma^0$. Using the frame (22) and exploring the representation in Eq. (24) and integrating over x we find

$$\int dx_v\, D^q(x_v, \gamma^0, v) = \frac{2}{v}\int d^4k \left(A_2^q + \frac{k^0}{M} A_3^q\right) = \frac{1}{v}\int dx\, f_1^q(x), \quad (27)$$

where again for symmetry reasons a term proportional to k^3 dropped out. The remaining integral coincides with that in Eq. (26) up to a prefactor of $1/v$, which is the expected velocity dependence for this sum rule; see Eq. (9).

We proceed analogously for $\Gamma = \gamma^3$. In the frame (22), we obtain after the x-integration of Eq. (25) the result

$$\int dx_v D^q(x_v, \gamma^3, v) = 2\int d^4k \left(A_2^q + \frac{k^0}{M} A_3^q\right) = \int dx\ f_1^q(x), \quad (28)$$

where again a term proportional to k^3 dropped out, and the resulting integral agrees with Eq. (26), which is velocity independent as expected for this sum rule; see Eq. (11).

The above derivations show that, if in a quark model the PDF flavor sum rule $\int_{-1}^{1} dx\, f_1^q(x) = N^q$ is fulfilled, then so are the sum rules (9), (11) for the QPDFs. It remains to be proven that the PDF complies with the quark flavor sum rule. This is done in Appendix B, where by evaluating the Dirac form factor $F_1^q(t)$ we show that $2\int d^4k (A_2^q + \frac{k^0}{M} A_3^q) = N^q$, which coincides with the above-encountered integral expressions and completes the proof.

F. Momentum sum rule

Next we investigate the second Mellin moment sum rule. For PDFs it corresponds to the momentum sum rule. For QPDFs there is no direct correspondence to momentum carried by partons, but we shall nevertheless loosely refer to

this sum rule by the same name. In the PDF case, we obtain from Eq. (24) the result

$$\int dx\, x\, f_1^q(x) = 2\int d^4k \left(\frac{k^0}{M}A_2^q + \frac{k_0^2+\frac{1}{3}\vec{k}^2}{M^2}A_3^q\right), \tag{29}$$

where terms proportional to $k^3A_2^q$ and $k^0k^3A_3^q$ dropped out for symmetry reasons. Moreover we use the fact that under the spatial part of the d^4k integral one can replace $(k^3)^2 \to \frac{1}{3}\vec{k}^2$ for symmetry reasons.

Having derived the result for the PDF, we now consider the QPDF in the case $\Gamma = \gamma^0$ in Eq. (24). After the x-integration, terms proportional to $k^3A_2^q$ and $k^0k^3A_3^q$ drop out also in this case, and we obtain

$$\int dx_v\, x_v\, D^q(x_v,\gamma^0,v) = \frac{2}{v}\int d^4k \left(\frac{k^0}{M}A_2^q + \frac{k_0^2+\frac{1}{3}\vec{k}^2}{M^2}A_3^q\right), \tag{30}$$

which corresponds to the result in Eq. (10) including the expected velocity dependence. After very similar steps, we obtain for the case $\Gamma = \gamma^3$ the result

$$\int dx_v\, x_v\, D^q(x_v,\gamma^3,v) = 2\int d^4k \left(\frac{k^0}{M}A_2^q + \frac{k_0^2+\frac{1}{3}\vec{k}^2}{M^2}A_3^q\right) - \frac{1-v^2}{v^2}\int d^4k \left(-\frac{2}{3}\frac{\vec{k}^2}{M^2}\right)A_3^q. \tag{31}$$

We recover the expected velocity dependence of the sum rule for $\Gamma = \gamma^3$ in agreement with Eq. (12).

In order to complete the proof, it is necessary to show that the above integral expressions correspond to the respective form factors of the energy-momentum tensor at zero-momentum transfer. This step is shown in Appendix C, which completes the proof of the sum rules (8), (10), (12) in quark models.

G. Proof of the Radyushkin formula

It is instructive to review the proof of Eq. (13) as formulated in Ref. [35] showing that it is a consequence of Lorentz invariance (the earlier proof [34] is based on a Nakanishi-type representation). The starting point is the correlator (14) projected on γ^μ in coordinate space representation. Let this correlator $C^\mu(P,z)$ be denoted as

$$\begin{aligned} C^\mu(P,z) &= \langle N|\bar{\Psi}^q(0)\gamma^\mu\Psi^q(z)|N\rangle \\ &= 2P^\mu\mathcal{M}^q(\nu,z^2) + 2z^\mu M^2\mathcal{J}^q(\nu,z^2), \\ \nu &= -P\cdot z, \end{aligned} \tag{32}$$

with the decomposition dictated by Lorentz invariance: the Lorentz index of $C^\mu(P,z)$ can be carried by the 4-vectors P^μ and z^μ, and the scalar amplitudes $\mathcal{M}^q$ and $\mathcal{J}^q$ can only be functions of $P\cdot z$ and z^2. The variable $\nu = -P\cdot z$ is called Ioffe time. The factor M^2 is introduced for convenience, such that $\mathcal{M}^q$ and $\mathcal{J}^q$ have the same dimension.

The PDF is defined by setting the index $\mu = +$ and $z^\mu = (0,\vec{0}_\perp,z^-)$ implying $\nu = -P^+z^-$ and $z^2 = 0$. The TMD is defined for $\mu = +$ and $z^\mu = (0,\vec{z}_\perp,z^-)$, which implies $\nu = -P^+z^-$ and $z^2 = -\vec{z}_\perp^2$. $D^q(x_v,\gamma^0,v)$ is defined for $z^\mu = (0,0,0,z^3)$ such that $\nu = P^3z^3$ or $z^3 = \nu/P^3$ and $z^2 = -\nu^2/P_3^2$. The definitions are given by [34,35]

$$\mathcal{M}^q(\nu,0) = \int_{-1}^{1} dx\, e^{i\nu x} f_1^q(x), \tag{33a}$$

$$\mathcal{M}^q(\nu,-\vec{z}_\perp^2) = \int_{-1}^{1} dx\, e^{i\nu x}\int d^2k_\perp\, e^{i\vec{k}_\perp\cdot\vec{z}_\perp} f_1^q(x,\vec{k}_\perp^2), \tag{33b}$$

$$\mathcal{M}^q\left(\nu,-\frac{\nu^2}{P_3^2}\right) = \int_{-\infty}^{\infty} dx_v\, e^{i\nu x_v} v D^q(x_v,\gamma^0,v). \tag{33c}$$

Notice that the Fourier transforms with respect to x in Eqs. (33a), (33b) have support only in the region $-1 < x < 1$. Inverting the Fourier transforms in Eqs. (33) yields

$$f_1^q(x) = \int_{-\infty}^{\infty}\frac{d\nu}{2\pi}e^{-i\nu x}\mathcal{M}^q(\nu,0), \tag{34a}$$

$$f_1^q(x,\vec{k}_\perp^2) = \int_{-\infty}^{\infty}\frac{d\nu}{2\pi}e^{-i\nu x}\int\frac{d^2z_\perp}{(2\pi)^2}e^{-i\vec{k}_\perp\cdot\vec{z}_\perp}\mathcal{M}^q(\nu,-\vec{z}_\perp^2), \tag{34b}$$

$$vD^q(x_v,\gamma^0,v) = \int_{-\infty}^{\infty}\frac{d\nu}{2\pi}e^{-i\nu x_v}\mathcal{M}^q\left(\nu,-\frac{\nu^2}{P_3^2}\right). \tag{34c}$$

The Radyushkin formula (13) can be derived as follows. For $\mathcal{M}^q(\nu,-\frac{\nu^2}{P_3^2})$ in Eq. (34c) one chooses the representation

$$\mathcal{M}^q\left(\nu,-\frac{\nu^2}{P_3^2}\right) = \mathcal{M}^q(\nu,-\vec{z}_\perp^2)\Big|_{\text{for }\vec{z}_\perp=(0,\frac{\nu}{P^3})}. \tag{35}$$

Inserting this representation in Eq. (34c) and carrying out the integrations over $d\nu$ and $d^2z_\perp$ yields Eq. (13) [35].

Several comments are in order. First, the amplitude $\mathcal{J}^q(\nu,z^2)$ is higher twist, and "it is better to get rid of it" [35]. It drops out in PDFs and TMDs automatically by focusing in $C^\mu(\nu,z^2)$ on the index $\mu = +$ while $z^+ = 0$. For QPDFs, $\mathcal{J}^q(\nu,z^2)$ drops out only for $\Gamma = \gamma^0$ when choosing $\mu = 0$ while $z^\mu = (0,0,0,z^3)$, but not in the case $\Gamma = \gamma^3$. Second, physically $z^3 = \frac{\nu}{P_3}$ and $\vec{z}_\perp$ are along different spatial directions, but Eq. (13) is mathematically correct independently of the physical meaning of the variables. We will check this below by an explicit model

calculation. Third, the factor of v in front of $D^q(x_v,\gamma^0,v)$ is due to different conventions in this work vs [34,35]; see Appendix A. Fourth, we recall that in QCD the TMD in (13) is defined with a straight gauge link and corresponds to a well-defined field theoretic object which can, e.g., be computed on the lattice but does not correspond to the TMDs that enter deep-inelastic processes. In contrast to this in quark models, where gauge links are absent, a regular (model) TMD enters in Eq. (13).

In order to prove the Radyushkin formula in our approach, we first need the expression for $f_1^q(x,\vec{k}_\perp^2)$ in terms of the $A_i^q = A_i^q(P\cdot k, k^2)$ amplitudes, which is given by

$$f_1^q(x,\vec{k}_\perp^2) = 2\int\int dk^0 dk^3 (A_2^q + xA_3^q)\delta\left(x - \frac{k^+}{P^+}\right), \tag{36}$$

where the dependence on $\vec{k}_\perp^2$ enters through the argument $k^2 = k_0^2 - \vec{k}_\perp^2 - k_3^2$ of the $A_i^q(P\cdot k, k^2)$ amplitudes. Inserting this expression in Eq. (13) yields

$$\begin{aligned} P_0\int_{-1}^1 dx \int_{-\infty}^\infty dk_1 f_1^q(x,k_1^2+(x_v-x)^2P_z^2) &= 2P_0\int_{-1}^1 dx \\ \times \int d^4k (A_2^q + xA_3^q)\delta\left(x-\frac{k^+}{P^+}\right)\delta(k^2-(x_v-x)P^3) &= \frac{2}{v} \\ \times \int d^4k \left(A_2^q + \frac{k^+}{P^+}A_3^q\right)\delta\left(x_v - \frac{k^+}{P^+} - \frac{k^2}{P^3}\right), \end{aligned} \tag{37}$$

where we implemented the condition that the transverse component k^2 in the TMD was fixed to the value $(x_v - x)P^3$ through integration over the δ-function $\delta(k^2-(x_v-x)P^3) = \frac{1}{P^3}\delta(x_v - \frac{k^+}{P^+} - \frac{k^2}{P^3})$ and used $v = \frac{P^3}{P^0}$.

The expression in Eq. (37) is the QPDF $D^q(x_v,v,\gamma^0,v)$ albeit not in the representation of Eq. (20) but in an equivalent representation. To demonstrate this, we follow some steps of the proof of Ref. [35]. For that we express the coordinate space correlator $C^\mu(P,z)$ in Eq. (32) through our momentum space amplitudes $A_i^q = A_i^q(P\cdot k, k^2)$. The former corresponds to the Fourier transform of the momentum space correlator in Eq. (18), such that we have

$$C^\mu(P,z) = 4\int d^4k e^{-ik\cdot z}(P^\mu A_2^q + k^\mu A_3^q). \tag{38}$$

Choosing for the Lorentz index $\mu = +$ and $z^\mu = (0,\vec{z}_\perp,z^-)$ the amplitude $\mathcal{J}^q$ drops out, see above, and we obtain for $\mathcal{M}^q(\nu,-\vec{z}^2)$ the representation

$$\mathcal{M}^q(\nu,-\vec{z}^2) = 2\int d^4k\, e^{i\nu\frac{k^+}{P^+}+i\vec{k}_\perp\cdot\vec{z}_\perp}\left(A_2^q + \frac{k^+}{P^+}A_3^q\right). \tag{39}$$

Choosing $\vec{z}_\perp = (0,\frac{\nu}{P_3})$ in Eq. (39) and inserting the so-obtained representation for $\mathcal{M}^q(\nu,-\frac{\nu^2}{P_3^2})$ in Eq. (34c) yields, after integrating over $d\nu$ and $d^2z_\perp$, the following equation:

$$D^q(x_v,\gamma^0,v) = \frac{2}{v}\int d^4k\left(A_2^q + \frac{k^+}{P^+}A_3^q\right)\delta\left(x_v - \frac{k^+}{P^+} - \frac{k^2}{P^3}\right). \tag{40}$$

Alternatively, setting $\mu = +$ and $z^\mu = (0,0,0,z^3)$ in (38) and plugging the so-obtained representation of $\mathcal{M}^q(\nu,-z_3^2)$ with $z^3 = \frac{\nu}{P^3}$ into Eq. (34c) yields the result in Eq. (20), demonstrating that the two expressions for $D^q(x_v,\gamma^0,v)$ in Eqs. (20) and (37) are equivalent, which completes the proof. While it is not an independent proof but rather an "adaptation" of the proof [35] to our momentum-space based approach, this shows that Eq. (13) must hold also in quark models. This presents an important cross-check for model computations.

In Ref. [35] it was concluded that Eq. (13) is based on Lorentz invariance. Since we describe $f_1^q(x,k_\perp^2)$ and $D^q(x_v,\gamma^0,v)$ in terms of manifestly Lorentz-invariant amplitudes $A_i^q(P\cdot k,k^2)$, one would think it should be possible to carry out the last step of our proof, namely the demonstration of the equivalence of the representations in Eqs. (20), (37) without the detour through the coordinate space representation of Ref. [35]. We tried hard but have not been able to find such a direct proof, which may indicate that exploring the coordinate space representation is an essential step.

H. Is the choice $\Gamma = \gamma^0$ or γ^3 preferable?

Formulations in coordinate and momentum space give complementary insights. It may therefore be instructive to investigate the question of which of the two choices is preferable from the perspectives of the $\mathcal{M}^q(\nu,z^2)$ and $\mathcal{J}^q(\nu,z^2)$ amplitudes as well as the $A_i^q(P\cdot k,k^2)$ amplitudes. Let us begin with the coordinate space representation. The expression for $D^q(x_v,\gamma^3,v)$ is obtained by choosing the index $\mu = 3$ in the correlator $C^\mu(P,z)$ in Eq. (32) and $z^\mu = (0,\vec{0}_\perp,z^3)$, where $\nu = -P\cdot z = P^3z^3$ or $z^3 = \frac{\nu}{P^3}$. In analogy to Eq. (33c), the QPDF $D^q(x_v,\gamma^3,v)$ is defined by

$$\begin{aligned} C^3(P,z) &= 2P^3\mathcal{M}^q(\nu,-z_3^2) + 2M^2z^3\mathcal{J}^q(\nu,-z_3^2) \\ &= 2P^3\int_{-\infty}^\infty dx_v\, e^{i\nu x_v}D^q(x_v,\gamma^3,v), \end{aligned} \tag{41}$$

which can be inverted and simplified using $z^3 = \frac{\nu}{P^3}$ as follows:

$$\begin{aligned} vD^q(x_v,\gamma^0,v) &= \int_{-\infty}^\infty \frac{d\nu}{2\pi}e^{-i\nu x_v}\mathcal{M}^q(\nu,-z_3^2) \\ D^q(x_v,\gamma^3,v) &= \int_{-\infty}^\infty \frac{d\nu}{2\pi}e^{-i\nu x_v}\left(\mathcal{M}^q(\nu,-z_3^2)\right. \\ &\quad \left. + \frac{M^2}{P_3^2}\nu\mathcal{J}^q(\nu,-z_3^2)\right), \end{aligned} \tag{42}$$

where we have included for comparison the result for $D^q(x_v,\gamma^0,v)$ discussed already in Sec. II G. Since $D^q(x_v,\gamma^3,v)$ contains the term $\frac{M^2}{P_3^2}\nu\mathcal{J}^q\times(\nu,-z_3^2)$ which is power-suppressed, the choice $\Gamma=\gamma^0$ appears preferable because in $D^q(x_v,\gamma^0,v)$ this power-suppressed term is absent to begin with [34,35].

To investigate this question from a momentum space perspective, we need to determine the explicit expressions for the amplitudes $\mathcal{M}^q(\nu,z^2)$ and $\mathcal{J}^q(\nu,z^2)$ from Eq. (38). The amplitude $A_2^q(P\cdot k,k^2)$ accompanied by the four-vector P^μ is readily Fourier transformed, giving a contribution $\mathcal{M}_1^q(\nu,z^2)$ to $\mathcal{M}^q(\nu,z^2)$. The amplitude $A_3^q(P\cdot k,k^2)$ is accompanied by the four-vector k^μ, which is the integration variable. Due to Lorentz invariance, the Fourier transform of this term contributes to $\mathcal{M}^q(\nu,z^2)$ a second contribution $\mathcal{M}_2^q(\nu,z^2)$ and gives rise to the amplitude $\mathcal{J}^q(\nu,z^2)$ according to

$$\begin{aligned}2\int d^4k e^{-ik\cdot z}k^\mu A_3^q(P\cdot k,k^2) &= P^\mu\mathcal{M}_2^q(\nu,z^2)\\ &\quad + z^\mu M^2\mathcal{J}^q(\nu,z^2),\\ \nu &= -P\cdot z.\end{aligned}\tag{43}$$

Contracting the above equation with the four-vectors P^μ and z^μ yields two equations for the two unknowns $\mathcal{M}_2^q(\nu,z^2)$ and $\mathcal{J}^q(\nu,z^2)$. Solving these equations [and adding $\mathcal{M}_1^q(\nu,z^2)$, which is just the Fourier transform of A_2^q] yields

$$\mathcal{M}^q(\nu,z^2)=2\int d^4k e^{-ik\cdot z}\left[A_2^q-\frac{(k\cdot z)\nu+(P\cdot k)z^2}{\nu^2+M^2z^2}A_3^q\right]\tag{44a}$$

$$\mathcal{J}^q(\nu,z^2)=2\int d^4k e^{-ik\cdot z}\left[-\frac{(P\cdot k)\nu+(k\cdot z)M^2}{M^2(\nu^2+M^2z^2)}A_3^q\right],\tag{44b}$$

where $A_i^q=A_i^q(P\cdot k,k^2)$. We make a first interesting observation. The amplitude $\mathcal{J}^q(\nu,z^2)$ receives a contribution from A_3^q just as $\mathcal{M}^q(\nu,z^2)$ does. Both A_2^q and A_3^q enter the description of the twist-2 PDF $f_1^q(x)$ in QCD and in models. In the parton model (or Wandzura-Wilczek approximation) where "interaction dependent" (so-called tilde) terms are neglected, the amplitude $A_2^q(P\cdot k,k^2)$ vanishes [78]. Thus, from this point of view, $\mathcal{J}^q(\nu,z^2)$ by itself does not appear to be any lesser than $\mathcal{M}^q(\nu,z^2)$. It merely appears with a power-suppressed prefactor.

Let us now inspect the two choices $D^q(x_v,\Gamma,v)$ in Eq. (42). Setting $z^\mu=(0,0,0,z^3)$ in Eq. (44) with $z^3=\frac{\nu}{P^3}$ and choosing $\Gamma=\gamma^0$ or γ^3 yields for ν-integrands of the two choices the following expressions in terms of A_i-amplitudes:

$$\Gamma=\gamma^0:\qquad \mathcal{M}^q\left(\nu,-\frac{\nu^2}{P_3^2}\right)=2\int d^4k\, e^{i\nu\frac{k^3}{P^3}}\left[A_2^q+\frac{\frac{k^3}{P^3}+\frac{P\cdot k}{P_3^2}}{1+\frac{M^2}{P_3^2}}A_3^q\right]\tag{45a}$$

$$\Gamma=\gamma^3:\qquad \mathcal{M}^q\left(\nu,-\frac{\nu^2}{P_3^2}\right)+\frac{M^2}{P_3^2}\nu\mathcal{J}^q(\nu,-z_3^2)=2\int d^4k e^{i\nu\frac{k^3}{P^3}}\underbrace{\left[A_2^q+\frac{\frac{k^3}{P^3}+\frac{P\cdot k}{P_3^2}}{1+\frac{M^2}{P_3^2}}A_3^q\right]}_{\mathcal{M}^q(\nu,-\frac{\nu^2}{P_3^2})}+\underbrace{\frac{\frac{k^3}{P^3}\frac{M^2}{P_3^2}-\frac{P\cdot k}{P_3^2}}{1+\frac{M^2}{P_3^2}}A_3^q}_{\frac{M^2}{P_3^2}\nu\mathcal{J}^q(\nu,-\frac{\nu^2}{P_3^2})}.\tag{45b}$$

The ratio $\frac{k^3}{P^3}$ corresponds to x_v, which asymptotically approaches x. The frame-independent factor $P\cdot k$ appears always in a ratio with respect to P_3^2, which makes it a power correction for $P^3\to\infty$. We also encounter power corrections of the type $\frac{M^2}{P_3^2}$. All these power corrections are evident in Eq. (45).

Now we make the second remarkable observation. The case $\Gamma=\gamma^0$ in Eq. (45a) stays as it is, while in the $\Gamma=\gamma^3$ case in Eq. (45b) all the power corrections mutually compensate, and we obtain

$$\Gamma=\gamma^3:\qquad \mathcal{M}^q\left(\nu,-\frac{\nu^2}{P_3^2}\right)+\frac{M^2}{P_3^2}\nu\mathcal{J}^q(\nu,-z_3^2)=2\int d^4k e^{i\nu\frac{k^3}{P^3}}\left[A_2^q+\frac{k^3}{P^3}A_3^q\right],\tag{45c}$$

which is rather remarkable. Inserting the results from Eq. (45) in Eq. (42) and taking the ν-integrals, we obtain

$$D^q(x_v,\gamma^0,v)=2\int d^4k\,\delta\left(x_v-\frac{k^3}{P^3}\right)\left[A_2^q+\frac{x_v+\frac{P\cdot k}{P_3^2}}{1+\frac{M^2}{P_3^2}}A_3^q\right]\sqrt{1+\frac{M^2}{P_3^2}}\tag{46a}$$

$$D^q(x_v,\gamma^3,v)=2\int d^4k\delta\left(x_v-\frac{k^3}{P^3}\right)[A_2^q+x_vA_3^q]. \quad (46b)$$

The expressions in Eq. (46) coincide with those in Eq. (20) as one can immediately see for $D^q(x_v,\gamma^3,v)$ and, after some algebra, also for $D^q(x_v,\gamma^0,v)$.

Several remarks are in order. The square-root factor in Eq. (46a) is $\frac{1}{v}$, cf. the end of Sec. II A, and can be avoided by using the conventions of Refs. [34,35] (see Appendix A) or by computing $vD^q(x_v,\gamma^0,v)$. The other power corrections cannot be avoided. Since the practical goal is to study the QPDFs at very large $P^3\gg M$ where the power corrections become small and QPDFs approach the PDF limit, there is a lot of practical interest to start with a representation of QPDFs which is more likely to exhibit faster convergence toward PDFs. Based on the coordinate space representation in Eqs. (42), the choice $\Gamma=\gamma^0$ appears more favorable because it avoids from the very beginning a power-correction term proportional to $J^q(\nu,-z_3^2)$. However, revisiting the situation in momentum space in terms of the $A_i^q(P\cdot k,k^2)$ amplitudes reveals that the inclusion of the power-correction term proportional to $\mathcal{J}^q(\nu,-z_3^2)$ in the case of $\Gamma=\gamma^3$ has actually a positive side effect: it cancels out power corrections present in the term proportional to $\mathcal{M}^q(\nu,-z_3^2)$ which remain uncompensated in $D^q(x_v,\gamma^0,v)$; see Eqs. (46). This in turn suggests that $D^q(x_v,\gamma^3,v)$ might be a better candidate for faster convergence toward PDFs.

The power corrections which enter in $D^q(x_v,\gamma^0,v)$ in Eq. (46a) and are absent in $D^q(x_v,\gamma^3,v)$ in Eq. (46b) are of the type $\frac{P\cdot k}{P_3^2}$ or $\frac{M^2}{P_3^2}$ and can be referred to as a type of kinematical or target-mass corrections. In addition to this, there are of course other, dynamical power corrections due to higher twist contributions which are not apparent in our approach. For instance, it is evident from the momentum sum rules, see Sec. II F, that $D^q(x_v,\gamma^3,v)$ contains a higher-twist contamination manifest through the energy-momentum tensor form factor $\bar{c}^q(0)$ which is twist-4 while the momentum sum rule of $D^q(x_v,\gamma^0,v)$ exhibits no such contamination. Nevertheless, as far as the simpler quark models are concerned, one may expect faster convergence for $\Gamma=\gamma^3$ than γ^0, although this remains to be asserted by explicit model calculations. For lattice fermion discretizations that break chiral symmetry, the γ^3 operator can mix with the scalar operator, whereas the γ^0 operator avoids this mixing and is therefore sometimes preferred in lattice-QCD calculations; see, e.g., Refs. [14,15,43,88–90].

The results and considerations presented thus far are valid for any quark model which respects Lorentz symmetry. In the next section we shall choose a specific model to illustrate and test the conclusions drawn in this section.

III. QPDFS IN THE COVARIANT PARTON MODEL

To present practical results we choose in this work the covariant parton model based on a systematic extension of Feynman's parton model concept [62,63] to the description of the partonic structure of hadrons [64–79].

A. Quark correlator, amplitudes, and PDFs in the CPM

Let us first briefly review the main results on the CPM [64–79] following the field-theoretic formulation of [77,78]. In the CPM, the partons are on shell, and the amplitudes A_i^q for $i=2,3$ needed for the unpolarized case are given by

$$\begin{aligned}
&A_2^q(P\cdot k,k^2)=0,\\
&A_3^q(P\cdot k,k^2)=M\delta(k^2-m_q^2)\Theta_{\rm kin}(P\cdot k)\mathcal{G}^q(P\cdot k),\\
&\Theta_{\rm kin}(P\cdot k)=\Theta_{\rm kin}^{(+)}(P\cdot k)+\Theta_{\rm kin}^{(-)}(P\cdot k),\\
&\Theta_{\rm kin}^{(\pm)}(P\cdot k)=\Theta(\pm P\cdot k)\Theta((P\mp k)^2),
\end{aligned} \quad (47)$$

where the Θ-functions ensure correct analytical properties [70,77] and the δ-function contains the on-shell condition. The vanishing of the amplitude A_2^q is a prediction of the parton model, although the same was observed also in some models with interactions [91]. The amplitude A_3^q is described in terms of the covariant function $\mathcal{G}^q(P\cdot k)$ which for $P\cdot k>0$ describes unpolarized quarks. For $P\cdot k<0$ it describes antiquarks via the relation $\mathcal{G}^{\bar{q}}(P\cdot k)=\mathcal{G}^q(-P\cdot k)$ [78]. The covariant functions $\mathcal{G}^a(P\cdot k)$ determine the unpolarized PDFs $f_1^a(x)$ for $a=q,\bar{q}$. In the nucleon rest frame and neglecting current quark mass effects, the unpolarized PDFs are given by

$$f_1^a(x)=2\pi xM^2\int_{\frac{1}{2}|x|M}^{\frac{1}{2}M}dk\,\mathcal{G}^a(Mk). \quad (48)$$

This one-to-one correspondence between $\mathcal{G}^a(P\cdot k)$ and $f_1^a(x)$ can be inverted to determine the covariant functions from a chosen input PDF parametrization according to

$$\mathcal{G}^a(P\cdot k)=-\frac{1}{\pi M^3}\left[\frac{d}{dx}\frac{f_1^a(x)}{x}\right]\Bigg|_{x=\frac{2P\cdot k}{M^2}},\qquad a=q,\bar{q}. \quad (49)$$

For massless partons, the variable $P\cdot k$ is constrained as $0<P\cdot k<\frac{1}{2}M^2$ due to the Θ-functions in Eq. (47). The choice of the renormalization scale μ of the input PDF in Eq. (49) is part of the modeling. The scale μ must be chosen to be several GeV, high enough for the parton model concept to be applicable. In an analogous way, it is possible to describe polarized PDFs and extend the approach to TMDs as well as subleading twist [64–79]. Notice that $f_1^a(x)/x$ is monotonically decreasing for all flavors in all parametrizations, which implies that $\mathcal{G}^a(P\cdot k)$ is positive.

B. Quasi-PDFs in the CPM

It is convenient to derive first the CPM expression for the QPDF with $\Gamma = \gamma^3$, which is a simpler case than $\Gamma = \gamma^0$. For that we insert the model results for the amplitudes (47) into Eq. (25), carry out the integration over dk^0 exploring $\delta(k^2 - m_q^2)$, and neglect m_q, which is appropriate for current masses of light quarks. This yields the results

$$D^q_\pm(x_v, \gamma^3, v) = 2x_v M \int \frac{d^3k}{2|\vec{k}|}\Theta(M - 2|\vec{k}|)\mathcal{G}^q(\pm M|\vec{k}|) \times \delta\left(\pm x_v - \frac{k^3 + v|\vec{k}|}{vM}\right), \tag{50}$$

where the $D^q_\pm(x_v, \gamma^3, v)$ denote the contributions due to, respectively, $\Theta^{(\pm)}_{\rm kin}(P\cdot k)$ in Eq. (47) which need to be added up to the total QPDF, but for now it is convenient to distinguish them for pedagogical purposes. In Eq. (50) for $D^q_\pm(x_v, \gamma^3, v)$ we substituted $k^3 \to (-k^3)$ under the d^3k integral. Setting $k^3 = |\vec{k}|\cos\vartheta$ and $k = |\vec{k}|$ and integrating in spherical coordinates over the angular variables $d\varphi d\cos\vartheta$, we obtain

$$D^q_\pm(x_v, \gamma^3, v) = 2\pi v x_v M^2 \int_{L_\pm(v)}^{\frac{1}{2}M} dk\, \mathcal{G}^q(\pm Mk), \qquad L_\pm(v) = \frac{v|x_v|M}{1 \pm v\,\mathrm{sign}(x_v)}. \tag{51}$$

In the case $\Gamma = \gamma^0$ we obtain in the same way the results

$$D^q_\pm(x_v, \gamma^0, v) = 2\pi M \int_{L_\pm(v)}^{\frac{1}{2}M} dk\, \mathcal{G}^q(\pm Mk)(x_v M v^2 \pm (1 - v^2)k). \tag{52}$$

The lower integration limits $L_\pm(v)$ in Eqs. (51), (52) arise from integrating the δ-function in Eq. (50) over $d\cos\vartheta$. The upper limit $\frac{1}{2}M$ can be traced back to the step functions in Eq. (47). The latter also ensure that $L_\pm(v) < \frac{1}{2}M$ and determine the support properties of QPDFs, which we will discuss in the next section. The final model results for the QPDF are given by

$$D^q(x_v, \Gamma, v) = D^q_+(x_v, \Gamma, v) + D^q_-(x_v, \Gamma, v). \tag{53}$$

In the limit $v \to 1$ when $x_v \to x$, the QPDFs approach

$$\lim_{v\to 1} D^q(x_v, \gamma^0, v) = \lim_{v\to 1} D^q(x_v, \gamma^3, v) = 2\pi x M^2 \int_{\frac{1}{2}|x|M}^{\frac{1}{2}M} dk \times \mathcal{G}^q(\mathrm{sign}(x)Mk) = f_1^q(x). \tag{54}$$

Considering the relation $\mathcal{G}^q(-P\cdot k) = \mathcal{G}^{\bar q}(P\cdot k)$ [78], we see that at negative x, Eq. (54) describes antiquark PDFs according to Eq. (5). The result in Eq. (54) agrees with the CPM expression for the unpolarized PDFs [73]. Hence, the CPM results for QPDFs have the correct limit (6).

C. Support properties of QPDFs and illustration with toy model input

It is interesting to investigate the support properties of QPDFs in the CPM in detail. As mentioned in Sec. III B, the step functions in Eq. (47) ensure that the lower and upper integration limits in Eqs. (51), (52) satisfy $L_\pm(v) < \frac{1}{2}M$. This condition determines the support properties of QPDFs. The total QPDF, Eq. (53), has nonzero support in a symmetric x_v interval, while the individual contributions $D^q_\pm(x_v, \Gamma, v)$ have support in asymmetric intervals as follows:

$$D^q(x_v, \Gamma, v) \neq 0 \ \text{ if } -\frac{1+v}{2v} \le x_v \le \frac{1+v}{2v} \ \xrightarrow{v\to 1}\ -1 < x < 1, \tag{55a}$$

$$D^q_+(x_v, \Gamma, v) \neq 0 \ \text{ if } -\frac{1-v}{2v} \le x_v \le \frac{1+v}{2v} \ \xrightarrow{v\to 1}\ 0 < x < 1, \tag{55b}$$

$$D^q_-(x_v, \Gamma, v) \neq 0 \ \text{ if } -\frac{1+v}{2v} \le x_v \le \frac{1-v}{2v} \ \xrightarrow{v\to 1}\ -1 < x < 0, \tag{55c}$$

where we indicate the limits $v \to 1$ when QPDFs become PDFs. These support properties imply that the one-to-one correspondence between PDFs $f_1^q(x)$ and covariant distributions $\mathcal{G}^a(P\cdot k)$ for $a = q, \bar q$, cf. Eqs. (48), (49) no longer holds for QPDFs. Instead, we find an interesting "leaking" phenomenon in the following sense.

For $v < 1$ the covariant distribution $\mathcal{G}^q(P\cdot k)$ determines $D^q_+(x_v, \Gamma, v)$, while $\mathcal{G}^{\bar q}(P\cdot k)$ determines $D^q_-(x_v, \Gamma, v)$. But the $D^q_\pm(x_v, \Gamma, v)$ contribute to both quark and antiquark QPDFs. As a consequence, the effects of the covariant quark distribution $\mathcal{G}^q(P\cdot k)$ (which for $v \to 1$ is solely responsible for the quark PDF) spill over into the antiquark region for $v < 1$ and vice versa; the effects of $\mathcal{G}^{\bar q}(P\cdot k)$ (which for $v \to 1$ is solely responsible for the antiquark PDF) leak into the antiquark region.

This leaking reflects the fact that a probabilistic parton density interpretation, and hence, distinction of quarks and antiquark degrees of freedom, requires the infinite momentum frame. In frames with $v < 1$ the distinction between quarks and antiquarks is lost. (In light cone quantization [92] a probabilistic interpretation can be given for any v.) When a nucleon moves with a velocity less than the speed of light (needed for a rigorous partonic interpretation in the infinite momentum frame), there are quark configurations inside the nucleon state which move in the opposite

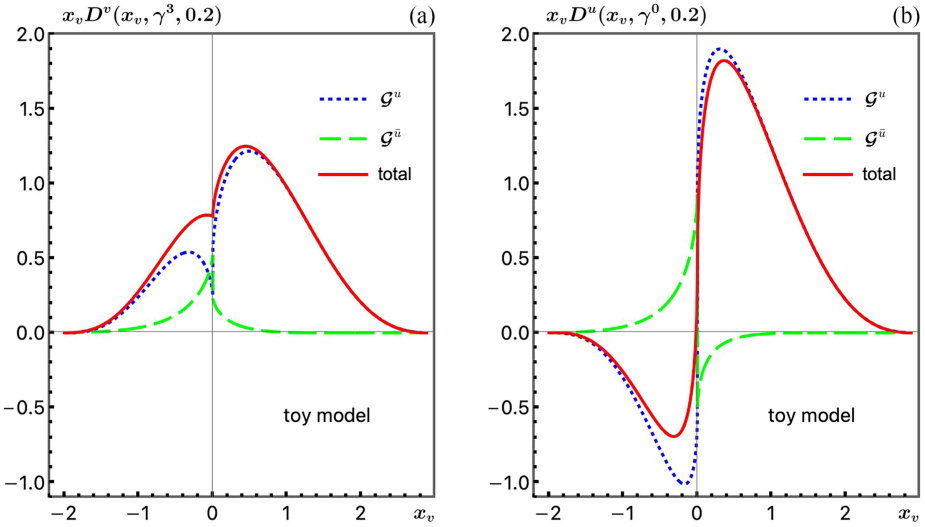


FIG. 1. The QPDFs for (a) the case $\Gamma = \gamma^3$ and (b) the case $\Gamma = \gamma^0$ as functions of x_v for $v = 0.2$ in the CPM based on toy model input for pedagogical purposes as described in the text. For $v = 1$ the covariant functions $\mathcal{G}^q(P \cdot k)$ and $\mathcal{G}^{\bar{q}}(P \cdot k)$ describe, respectively, the quark PDF and antiquark PDFs. For $v < 1$ the effects of quarks described in terms of $\mathcal{G}^q(P \cdot k)$ "leak" into the antiquark region, and the effects of antiquarks described by $\mathcal{G}^{\bar{q}}(P \cdot k)$ leak into the quark region.

direction and "mimic" antiquarks [5]. This corresponds in the CPM to the leaking of $D^q_+(x_v, \Gamma, v)$ into negative x_v. Similarly, antiquark configurations exist for $v < 1$ in the nucleon state which move in the opposite direction to the nucleon, mimicking quarks [5]. This corresponds in the CPM to the leaking of $D^q_-(x_v, \Gamma, v)$ into positive x_v.

In Fig. 1 we illustrate the leaking phenomenon using toy model PDFs as input, which behave like $f_1^a(x) \propto 1/x$ at small x. This has the advantage that $D^a(x_v, \Gamma, v) \propto 1/x_v$ at small x_v such that there is no singularity at $x_v = 0$ when plotting $x_v D^a(x_v, \Gamma, v)$ over the entire x_v interval. The toy model PDFs are used only in this section to demonstrate generic features. The small-x_v behavior of QPDFs in the CPM for any input PDFs will be discussed in Sec. III F, and numerical results from realistic parametrizations will be shown in Sec. IV.

For pedagogical purposes, we focus on u-flavor and determine the CPM covariant functions $\mathcal{G}^a(P \cdot k)$ in Eq. (49) from analytical toy model PDFs defined as $f_1^a(x) = A_a x^{-B_a}(1 + C_a x^{1/2} + D_a x)(1 - x)^{E_a}$ with the parameters $A = A_u = A_{\bar{u}} = 0.3$, $B = B_u = B_{\bar{u}} = 1.0$, $C_u = 3.0$, $C_{\bar{u}} = -1.6$, $D_u = 10.0$, $D_{\bar{u}} = 1.25$, $E_u = 3.0$, $E_{\bar{u}} = 5.0$. This toy model is not unrealistic and is chosen such that for $0.01 \lesssim x \lesssim 0.7$ it approximates the NLO LHAPDF parametrization from [93] at the scale $\mu^2 = 4\ \mathrm{GeV}^2$ within a few percent accuracy and accurately reproduces the first two Mellin moments. Notice that the parameters $A = A_a$ and $B = B_a < 2$ must be the same for $a = q, \bar{q}$ for the sum rules to be convergent (as is the case also for realistic PDFs). For $x \lesssim 10^{-2}$ we deliberately choose to deviate from realistic PDFs for pedagogical reasons, and the large-x region is of no relevance for the purposes of this section.

For the relatively low nucleon velocity $v = 0.2$ chosen in Fig. 1, which corresponds to $P_z = 0.19$ GeV, the support of $D^q_+(x_v, \Gamma, v)$ is the region $-2 \le x_v \le 3$, while that of $D^q_-(x_v, \Gamma, v)$ is the region $-3 \le x_v \le 2$. It is a general feature of the CPM that for lower v, the QPDFs spread further beyond the PDF support region $|x| < 1$; see Eqs. (55a)–(55b). (Another general feature worth mentioning in passing is that QPDFs diverge in the opposite limit, $v \to 0$.)

In Fig. 1(a) we see that for low velocities, $D^q_+(x_v, \gamma^3, v)$ [which would provide the sole contribution to $f_1^q(x)$ for $v \to 1$] leaks so significantly into the negative x_v that $D^q_+(x_v, \gamma^3, v)$ is the dominant contribution in this region. The effect is mutual, and $D^q_-(x_v, \gamma^3, v)$ (responsible for the sole contribution to the antiquark PDF for $v \to 1$) leaks into positive x_v but has there a much smaller effect and constitutes a modest correction to the total QPDF. The contributions of $x_v D^q_\pm(x_v, \gamma^3, v)$ to the total QPDF in all x_v-regions are always positive and add up.

In Fig. 1(b) in the case $\Gamma = \gamma^0$ we also observe a significant leaking of $x_v D^q_+(x_v, \gamma^0, v)$ into the negative x_v-region and less pronounced leaking of $x_v D^q_-(x_v, \gamma^0, v)$ into positive x_v. But the leaking pattern is fundamentally different in the two cases: for $\Gamma = \gamma^0$ the respective "leaking-in" contributions have opposite signs and lead to cancellations; see Fig. 1(b). In our case (which is realistic for that matter) at lower velocities the cancellation in the negative x_v-region is so strong that it reverses the sign of the QPDF. Whether or not, in the case of $\Gamma = \gamma^0$, the leaking of $x_v D^q_+(x_v, \gamma^0, v)$ into the negative x_v-region is strong enough for $x_v D^q_+(x_v, \gamma^0, v)$ to dominate over $x_v D^q_-(x_v, \gamma^0, v)$ and reverse the sign of the total QPDF,

depends on the input PDFs. This is generally the case for PDFs where $xf_1^q(x)$ has a pronounced maximum in the valence x-region as is the case with more or less realistic u- and d-flavor PDFs as input.[1] As v increases, the magnitude of the sign-reversing leaking-in contribution to the antiquark QPDF decreases.

D. Sum rules for QPDFs in the CPM

In order to prove that the sum rules in the CPM, we first derive the model expressions for the form factors $F_1^q(0)$, $A^q(0)$, $\bar{c}^q(0)$. Evaluating the general quark model expressions for these form factors derived in Appendixes B and C, we obtain the results

$$F_1^q(0) = 2\int d^4k \frac{E_q}{M} A_3^q, \qquad E_q = \sqrt{\vec{k}^2 + m_q^2}, \tag{56}$$

$$A^q(0) = 2\int d^4k \left(\frac{4}{3}\frac{\vec{k}^2}{M^2} + \frac{m_q^2}{M^2}\right) A_3^q, \tag{57}$$

$$\bar{c}^q(0) = 2\int d^4k \left(-\frac{1}{3}\frac{\vec{k}^2}{M^2}\right) A_3^q, \tag{58}$$

where E_q is the energy of the on-shell partons, and we keep track of current quark mass effects.

Interestingly, in the CPM the form factors $A^q(0)$ and $\bar{c}^q(0)$ are related modulo current quark mass effects. By exploring the δ-function $\delta(k^2 - m_q^2)$ inherent in A_3^q in Eq. (47), we obtain from Eqs. (57), (58)

$$A^q(0) = -4\bar{c}^q(0) + \frac{2m_q^2}{M^2}\int d^4k\, A_3^q. \tag{59}$$

For light quarks $m_q^2 \ll M^2$, the CPM practically predicts the relation

$$\bar{c}^q(0) = -\frac{1}{4}A^q(0) \quad \text{(CPM)}. \tag{60}$$

This is a benchmark result in the sense that Eq. (60) is based purely on Lorentz symmetry and free field theory. The CPM has been argued [94] to be practically equivalent to the Wandzura-Wilczek (WW) approximation in QCD where quark-gluon correlators are systematically neglected with respect to quark correlators; see, e.g., [95]. Hence, our result, Eq. (60), can be more broadly viewed as a prediction of the WW approximation.

When interactions are present, one can in general expect deviations from (60), and it is instructive to compare to results from other approaches. Remarkably, the relation (60) holds exactly in the bag model like in the CPM (provided $m_q = 0$ is set in both cases), albeit the bag model result refers to a low hadronic scale [96–98]. Interestingly, in the bag model there is a "gluon" contribution (mimicked by the bag) given by $\bar{c}^g(t) = -\sum_q \bar{c}^q(t)$ with $\bar{c}^g(0) = \frac{1}{4}$ for $m_q = 0$ [97]. The reason why (60) holds in the bag model may presumably be due to the quarks inside the bag obeying the free Dirac equation, as they do in the CPM, but this point may deserve more model studies. The chiral quark soliton model offers a different scenario where the quarks obey a Dirac equation coupled to a strong mean ("soliton") field. This leads to a very different prediction, namely $\bar{c}^{u+d}(0) = 0$ [99] in distinction to (60). Notice that the separate u- and d-flavor results are nonzero with $\bar{c}^u(0) = -\bar{c}^d(0) = 0.04$ at a low scale $\mu^2 \sim 0.4$ GeV^2 [100]. The instanton vacuum model predicts $\bar{c}^{u+d}(0) = 0.014$ also at $\mu^2 \sim 0.4$ GeV^2 [101]. We note these results refer to low scales while the CPM is defined at higher scales, so the above comparison is qualitative.

For a more quantitative comparison, we resort to results from the literature referring to higher scales [102,103] where, respectively, the value $\sum_q \bar{c}^q(0) = -0.11$ was obtained phenomenologically [102] and the value -0.12 from the lattice QCD calculation [103]. These results refer to summation over the light flavors $q = u, d, s$ and the renormalization scale $\mu^2 = 4$ GeV^2. Choosing as input for the CPM the NLO LHAPDFA parametrization [93] at $\mu^2 = 4$ GeV^2, where $A^u(0) = 0.347$, $A^d(0) = 0.195$, $A^s(0) = 0.032$, we obtain the estimate $\sum_q \bar{c}^q(0) = -0.14$, which agrees within 20% with [102,103]; i.e., for this property and at this scale the WW approximation works reasonably well. This is indeed within the accuracy of the WW approximation in QCD as inferred phenomenologically for the twist-3 PDF $g_T^a(x)$ [104].

At first glance, one might hope to observe a better agreement at higher scales where the parton model picture is better justified (we recall that the choice of scale is part of modeling in the CPM; see Sec. III A). Interestingly, this is not the case. In Ref. [105] the QCD evolution properties of $\bar{c}^q(0)$ were studied, and the asymptotic limit was derived [the notation is $\bar{c}^q(t, \mu^2)$, but throughout we omit the scale dependence for brevity, and the result below refers to $t = 0$]:

$$\lim_{\mu^2\to\infty} \sum_q \bar{c}^q(0) = -\frac{1}{4}\lim_{\mu^2\to\infty}\sum_q A^q(0) - \frac{N_f}{6\beta_0}, \tag{61}$$

where $\lim_{\mu^2\to\infty}\sum_q A^q(0) = N_f/(N_f + 4C_F)$ with $C_F = (N_c^2 - 1)/(2N_c)$. Here, N_c is the number of colors in QCD,

[1] In a less realistic toy model $f_{\text{toy}}^a(x) = Ax^{-1}(1-x)^{B_a}$ with $B_q = 4$ and $B_{\bar{q}} = 8$ with A fixed by the flavor number sum rule, the resulting leaking of $x_v D_+^q(x, \gamma^0, v)$ does not overwhelm $x_v D_-^q(x, \gamma^0, v)$ for $x_v < 0$, and the total $x_v D^q(x, \gamma^0, v)$ is positive throughout. The reason why in this case the leaking pattern is unlike in Fig. 1(b) is because, in this toy model, $xf_{\text{toy}}^q(x)$ has no maximum. The reversal of the sign of $x_v D^q(x, \gamma^0, v)$ at $x_v < 0$ for low and moderate velocities requires a pronounced valence behavior of $xf_1^q(x)$.

and $\beta_0 = \frac{11}{3} C_A - \frac{2}{3} N_f$ is the leading coefficient of the QCD β-function and $C_A = N_c$. For $N_f = 3$ flavors the asymptotic QCD formula (61) yields $\lim_{\mu^2\to\infty} \sum_q \bar{c}^q(0) = -0.15$ while the CPM yields -0.09. The discrepancy is due to the piece $-N_f/(6\beta_0)$ in Eq. (61). which arises from the trace anomaly in QCD. It is not surprising to miss out on effects of quantum anomalies in a parton model framework where one neglects (quantum) interactions in the first place. Still, the asymptotic CPM and QCD results agree within 40%. Combining with what we learned in the previous paragraph from the comparison to Refs. [102,103], we conclude that the CPM prediction for $\bar{c}^q(0)$ works within (20–40)%. Incidentally, this is an "accuracy" one often observes in model studies. The numerical values of $A^q(0)$ and $\bar{c}^q(0)$ are of importance for the decomposition of hadron masses in QCD [106–109].

E. Further general properties of QPDFs in the CPM

In this section, we discuss several general properties of QPDFs in the CPM. One interesting general feature in the CPM is that $D^q(x_v, \gamma^3, v)$ and $D^{\bar{q}}(x_v, \gamma^3, v)$ are always positive for all velocities $0 < v \le 1$; i.e., the CPM predicts

$$D^a(x_v, \gamma^3, v) \ge 0, \qquad a = q, \bar{q}, \qquad 0 < v \le 1. \quad (62)$$

This is true in the CPM for any input PDF; i.e., it is not specific to using toy model or realistic PDFs as input. The result in Eq. (62) follows from the positivity of the covariant functions $\mathcal{G}^a(P\cdot k)$ for $a = q, \bar{q}$, which follows from the positivity of $f_1^a(x)$ via Eq. (49). Notice that the positivity of $f_1^a(x)$ is obvious in the parton model framework or at tree level in QCD, but cannot be proven in general in QCD [110]. Within the simpler framework of the CPM, the positivity of $D^a(x_v, \gamma^3, v)$ in Eq. (62) is a rigorous result.

Another interesting generic property in the CPM is that the contributions $D^q_\pm(x_v, \Gamma, v)$ to the two representations for $\Gamma = \gamma^0$ and $\Gamma = \gamma^3$ are related to each other, according to Eqs. (51), (52), as

$$D^q_\pm(x_v, \gamma^0, v) = v D^q_\pm(x_v, \gamma^3, v) + \Delta D^q_\pm(x_v, v)$$
$$\Delta D^q_\pm(x_v, v) = \pm(1-v^2) 2\pi M \int_{L_\pm(v)}^{\frac{1}{2}M} dk\, k\, \mathcal{G}^q(\pm Mk), \quad (63)$$

and the corresponding total QPDFs are related analogously, according to Eq. (53). This relation is very interesting. It shows that $D^q(x_v, \gamma^0, v)$ contains the expression for $D^q(x_v, \gamma^3, v)$ "diluted" by an additional power of nucleon velocity and "contaminated" by the extra term $\Delta D^q_\pm(x_v, v)$ proportional to $(1 - v^2)$. Based on the model expressions alone, it is not possible to tell which choice, $\Gamma = \gamma^0$ or γ^3, may converge faster, and we have to postpone this question until the numerical study.

The "extra term" $\Delta D^q_\pm(x_v, v)$ in Eq. (63) is interesting for several reasons. First, this term is the reason why there is no positivity property for $D^q_\pm(x_v, \gamma^0, v)$ at $v < 1$ unlike for $D^q_\pm(x_v, \gamma^3, v)$ in Eq. (62). Second, it causes a different leaking behavior in the cases $\Gamma = \gamma^0$ and $\Gamma = \gamma^3$ as we observed in Sec. III C. If we read Eq. (63) the other way round as $v D^q_\pm(x_v, \gamma^3, v) = D^q_\pm(x_v, \gamma^0, v) - \Delta D^q_\pm(x_v, v)$, then we recognize a third feature, namely $\Delta D^q_\pm(x_v, v)$ is responsible for the contribution of $\bar{c}^q(t)$ in the sum rule in Eq. (12), which is genuinely twist-4. In fact, this term comes with the prefactor $(1 - v^2) = M^2/(M^2 + P_3^2)$, which corresponds for $P^3 \gg M$ to a power suppression of $\mathcal{O}(\frac{M^2}{P_3^2})$.

Notice that "reading Eq. (63) in another way" above was necessary to reconcile with the general sum rule (12). But in the model this "twist-4" piece actually explicitly appears as an additional term in $D^q_\pm(x_v, \gamma^0, v)$ and not in $D^q_\pm(x_v, \gamma^3, v)$, which is another interesting observation. Where the power corrections appear may depend on the point of view; see the discussion of power corrections in coordinate vs momentum space in Sec. II H. It would be very interesting to investigate this point further in other models.

In lattice QCD calculations, the mixing with twist-4 contributions makes the studies of $D^q(x_v, \gamma^3, v)$ more involved compared to $D^q(x_v, \gamma^0, v)$. In the CPM, all twists are described on equal footing (within the WW-type approximation), and there is *a priori* no preference to favor $\Gamma = \gamma^0$ or $\Gamma = \gamma^3$.

F. Small-x_v behavior of QPDFs in the CPM

The small-x behavior of PDFs determines the small-x_v behavior of QPDFs. The connection can be derived analytically in the CPM as follows. Let a PDF have the small-x behavior

$$f_1^a(x) = A x^{-B} + \ldots \quad \text{for } x \to 0, \quad a = q, \bar{q}, \quad (64)$$

where the dots denote subleading terms. The constants A and B are positive and scale and flavor dependent, which we do not indicate for notational brevity. Based on Eq. (49) the covariant function exhibits the behavior

$$\mathcal{G}^a(P\cdot k) = \frac{A(B+1)}{\pi M^3} \left(\frac{2P\cdot k}{M^2}\right)^{-B-2} + \ldots \quad \text{for } P\cdot k \to 0, \quad (65)$$

i.e., the covariant functions diverge strongly for $P\cdot k \to 0$. These properties imply for the QPDFs the small-x_v behavior

$$D^a(x_v, \Gamma, v) = C(\Gamma, v) A x_v^{-B} + \ldots \quad \text{for } x_v \ll \frac{1-v}{2v}, \quad (66)$$

with the velocity dependent coefficients (for $0 < v \le 1$ and $B \ne 0$, for realistic parametrizations $1 < B < 2$)

$$C(\gamma^3, v) = v\left[\left(\frac{1+v}{2v}\right)^{B+1} + \left(\frac{1-v}{2v}\right)^{B+1}\right],$$
$$C(\gamma^0, v) = vC(\gamma^3, v) + (1-v^2)\frac{B+1}{2B} \times \left[\left(\frac{1+v}{2v}\right)^{B} - \left(\frac{1-v}{2v}\right)^{B}\right]. \quad (67)$$

Both coefficients have the property $\lim_{v\to 1} C(\Gamma, v) = 1$, and we recover the correct small-x behavior (64) of the PDF for $v \to 1$. The results (66), (67) can be viewed as predictions of the WW-type approximation.

G. Large-x_v behavior of QPDFs in the CPM

Also the large-x_v behavior of QPDFs can be derived analytically in the CPM. Let us recall, cf. Eq. (55), that in the CPM the QPDFs vanish for $x_v \geq x_{v,\max}$ with the definition

$$x_{v,\max} = \frac{1+v}{2v}, \quad (68)$$

which is larger than unity for $0 < v < 1$ and $\lim_{v\to 1} x_{v,\max} = 1$. This is notably different from QCD and the models we are aware of where the support of QPDFs extends to infinity. For $x_v \to x_{v,\max}$ the behavior of the QPDFs in the CPM can be derived analytically analogously to Sec. III F. Let the large-x behavior of a PDF be given by

$$f_1^a(x) = c_L(1-x)^N + \ldots \quad \text{for } x \to 1, \quad (69)$$

where the dots denote subleading terms. The constants c_L and N differ for each parton species $a = u, \bar{u}, d, \bar{d}, \ldots$ and are scale dependent and positive. The covariant functions $\mathcal{G}^a(P\cdot k)$ vanish (for massless partons) for $2P\cdot k \geq M^2$ based on the constraints encoded in the Θ-functions in Eq. (47), and the large-x behavior of the PDFs implies that

$$\mathcal{G}^a(P\cdot k) = \frac{c_L N}{\pi M^3}\left(1 - \frac{2P\cdot k}{M^2}\right)^{N-1} + \ldots \quad \text{for } 2P\cdot k \to M^2. \quad (70)$$

This in turn implies for QPDFs the large-x_v behavior [note that vx_v below approaches $\frac{1}{2}(1+v) + \cdots$ for $x_v \to x_{v,\max}$]

$$D^a(x_v, \Gamma, v) = c_L v x_v\left(1 - \frac{x_v}{x_{v,\max}}\right)^N + \ldots, \qquad \Gamma = \gamma^0, \gamma^3. \quad (71)$$

Interestingly, both choices $\Gamma = \gamma^0, \gamma^3$ exhibit the same large-x_v behavior and are larger than the PDF at large x_v. The same behavior was observed in prior model studies [53–56].

TABLE I. Nucleon velocities v and momenta P_z chosen for displaying numerical results along with the QPDF support $0 \leq x_v \leq x_{v,\max}$ in the CPM ($v = 0.2$ is used only in Fig. 1 and for pedagogical purposes).

Nucleon velocity v	0.2	0.5	0.7	0.9	1
Nucleon momentum P_z [GeV]	0.19	0.54	0.92	1.94	∞
Range of QPDF support $x_{v,\max}$	3	1.5	1.21	1.06	1

IV. NUMERICAL RESULTS FOR QPDFS IN CPM

We determine the covariant functions $\mathcal{G}^a(P\cdot k)$ in Eq. (49) using the NLO LHAPDF parametrization [93] at $\mu^2 = 4$ GeV^2 for $a = u, d, \bar{u}, \bar{d}, s$ and compute the CPM results for $D^a(x_v, \Gamma, v)$ based on Eqs. (51)–(53). Since $f_1^s(x) = f_1^{\bar{s}}(x)$ in the parametrization [93], also the pertinent QPDFs coincide, and we show results for only one of them.

In order to demonstrate the convergence of the QPDFs we choose the velocities $v = 0.5, 0.7, 0.9$, which correspond to nucleon momenta P_z as shown in Table I. For these velocities, in the CPM the QPDFs have nonzero support for $0 < x_v < x_{v,\max}$ with $x_{v,\max}$ as shown in Table I. Unlike in Fig. 1, the antiquark PDFs will be displayed for positive x_v [recall that Eq. (5) allows one to switch back and forth between these equivalent displays].

A. CPM results for $x_v D^a(x_v, \Gamma, v)$

In Fig. 2 we show results for $x_v D^a(x_v, \gamma^0, v)$ from the CPM obtained in the above described way. It is of advantage to show $x_v D^a(x_v, \Gamma, v)$ rather than the QPDFs themselves to suppress their strong rise at small x_v, and the curves are plotted for positive $x_v \geq 10^{-2}$. The region of smaller x_v (omitted in Fig. 2) will be discussed in detail in Sec. IV C. Notice that for the quark flavors u and d in the upper panel of Fig. 2, we use a different scale than for the sea quarks $\bar{u}$, $\bar{d}$, $s = \bar{s}$ in the lower panel of Fig. 2.

For the selected velocities, the convergence of the QPDFs toward the corresponding PDFs is relatively uniform. The only exception is $x_v D^{\bar{u}}(x_v, \gamma^0, v)$ at the velocity $v = 0.5$, which shows a "wiggle" for $x_v \lesssim 0.3$. This is a "remnant" of the opposite-sign leaking phenomenon manifest for $x_v D^a(x_v, \gamma^0, v)$ at still lower velocities $v \lesssim 0.3$, which was shown in Fig. 1(b) and discussed in detail in Sec. III C. In particular, it is worth noticing that for $v = 0.9$ the QPDFs agree with the PDFs for $10^{-2} \lesssim x_v \lesssim 0.8$ already within about 5% accuracy. In QCD and other quark models a slower convergence is observed. This indicates the impact of off-shellness effects for the convergence of QPDFs.

In Fig. 3 we show the analogous CPM results for $x_v D^a(x_v, \gamma^3, v)$ displaying also in this case only the region of $x_v \geq 10^{-2}$ and postponing the discussion of the region of smaller x_v for Sec. III F. Notice that also in this figure we

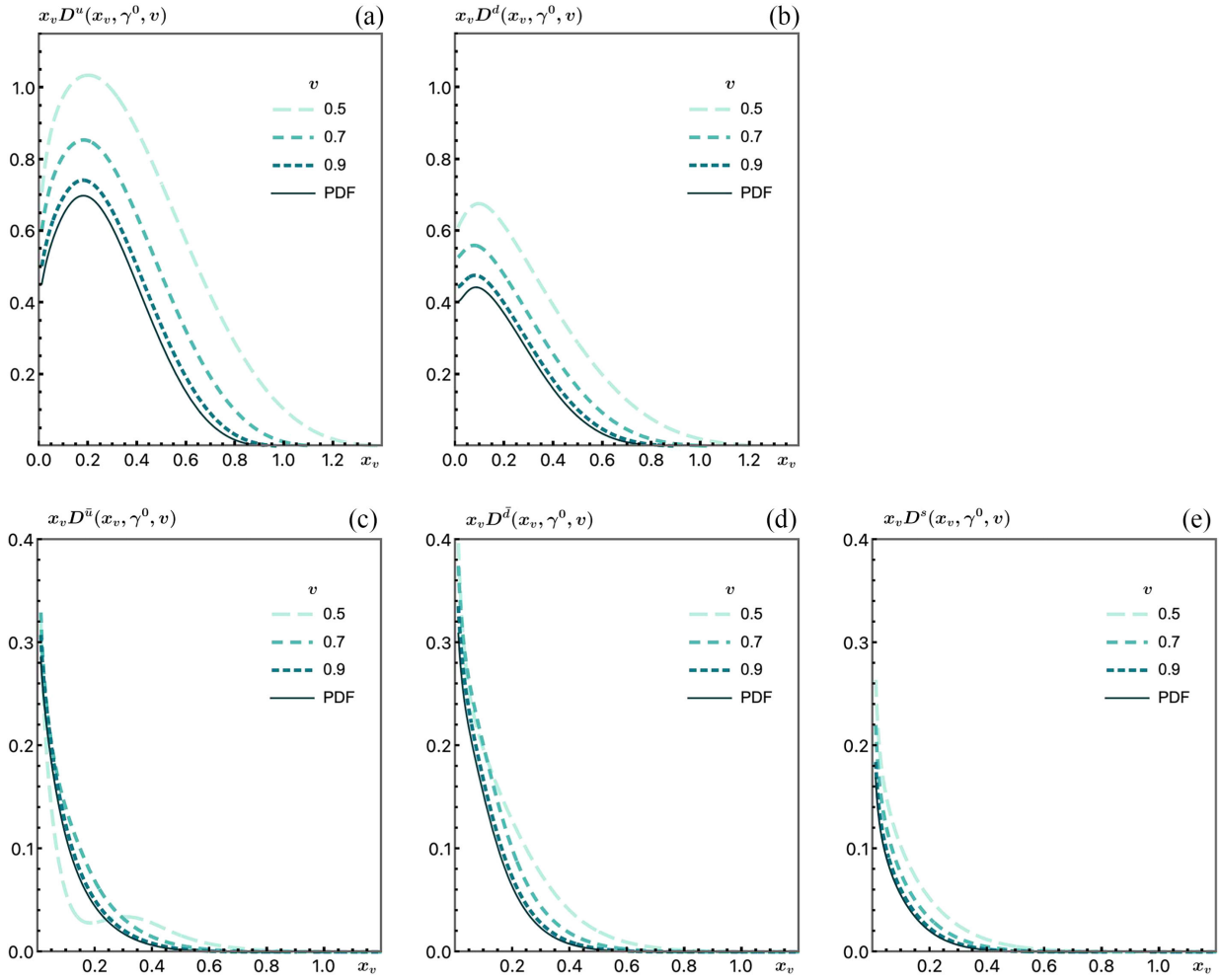


FIG. 2. The QPDFs $x_v D^a(x_v, \gamma^0, v)$ in the CPM as functions of $x_v \geq 10^{-2}$ at the scale $\mu^2 = 4$ GeV^2 for the quark flavors $a = u, d$ [upper panel (a) and (b)] and sea quarks $\bar{u}, \bar{d}, s$ [lower panel (c)–(e)] based on the NLO PDF parametrization [93]. We show QPDFs for the velocities $v = 0.5, 0.7, 0.9$ and include the PDFs for comparison.

use different scales for the quark QPDFs in the upper panel and the antiquark QPDFs in the lower panel. We use the same velocities as in the case $\Gamma = \gamma^0$ in Fig. 2, namely $v = 0.5,\ 0.7,\ 0.9$ and observe an even more uniform convergence toward the PDFs compared to the $\Gamma = \gamma^0$ case.

One interesting observation is that as the limit $v \to 1$ is approached, in the region $10^{-2} \leq x_v \lesssim 0.2$, the quark QPDFs $x_v D^q(x_v, \gamma^3, v)$ for $q = u, d$ converge faster toward the corresponding PDFs than the $x_v D^q(x_v, \gamma^0, v)$. Hereby we also notice an interesting flavor dependence with $x_v D^u(x_v, \gamma^3, v)$ converging toward $x f_1^u(x)$ faster than $x_v D^d(x_v, \gamma^3, v)$ converging toward $x f_1^d(x)$; cf. Figs. 3(a) and 3(b). The latter observation can be explained by the leaking phenomenon discussed in Sec. III C. In the case $\Gamma = \gamma^3$ the leaking occurs with the same sign, but it is important to recall the sea quark flavor asymmetry $f_1^{\bar{d}}(x) > f_1^{\bar{u}}(x)$, while for quarks we have the opposite situation with $f_1^u(x) > f_1^d(x)$. Therefore, the leaking effect of the larger $\bar{d}$-antiquark contribution on the smaller d-quark QPDF is more pronounced than in the u-flavor case, which causes a slower convergence. It will be interesting to see if this trend can also be seen in other quark models and lattice QCD studies.

It is also noteworthy that we do not observe any wiggles in $x_v D^a(x_v, \gamma^3, v)$ which converge uniformly toward the corresponding PDFs as v approaches unity (to be contrasted with the case for $\Gamma = \gamma^0$ as evident for $\bar{u}$ at $x_v = 0.5$). It is instructive to compare the two cases $\Gamma = \gamma^0$ and γ^3 more quantitatively, which we do in Sec. IV B.

B. Comparison of the $\Gamma = \gamma^0$ vs γ^3 cases

In Fig. 4 we present a direct comparison of the cases $\Gamma = \gamma^0$ and γ^3 at the selected velocities $v = 0.5, 0.7, 0.9$, including the respective PDFs for comparison. Hereby we limit ourselves to the u-quark QPDFs in Figs. 4(a)–4(c) and omit the d-quark QPDFs, which look qualitatively very similar. We also limit ourselves to showing the $\bar{u}$-antiquark

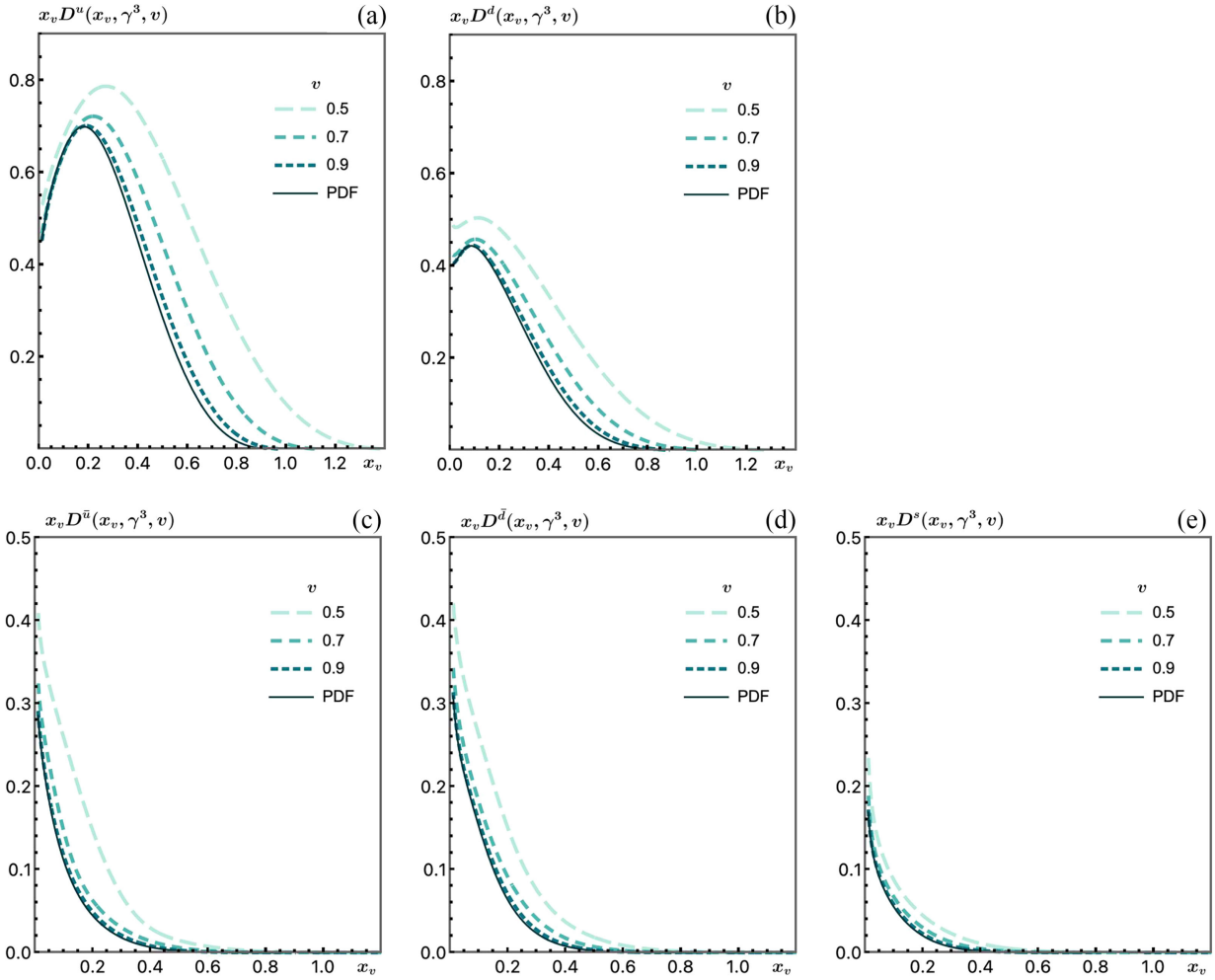


FIG. 3. The QPDFs $x_v D^a(x_v, \gamma^3, v)$ in the CPM as functions of $x_v \geq 10^{-2}$ at the scale $\mu^2 = 4$ GeV^2 for the quark flavors $a = u$, d [upper panel (a) and (b)] and sea quarks $\bar{u}, \bar{d}, s$ [lower panel (c)–(e)] based on the NLO PDF parametrization [93]. We show QPDFs for the velocities $v = 0.5$, 0.7, 0.9 and include the PDFs for comparison.

QPDFs in Figs. 4(d)–4(f) representatively for other sea quark QPDFs, which exhibit similar patterns.

Let us discuss first the quark case. It is an interesting observation that in the region of larger x_v the two choices $\Gamma = \gamma^0$ and γ^3 give basically the same result. What larger x_v means depends, hereby, on the velocity. On the scale of Figs. 4(a)–4(c), for $v = 0.5$ the two curves for $\Gamma = \gamma^0$ and γ^3 can hardly be distinguished for $x_v \gtrsim 0.9$. When $v = 0.7$, this happens for $x_v \gtrsim 0.65$, and for $v = 0.9$, the two curves become hardly distinguishable in the region of $x_v \gtrsim 0.45$. Remarkably, while the curves for $\Gamma = \gamma^0$ and γ^3 agree between them at larger x_v, even at $v = 0.9$ they systematically disagree with the PDF.

Another remarkable observation is that the convergence of $x_v D^u(x_v, \gamma^0, v)$ is relatively uniform over the entire x_v region; see the upper panel of Fig. 4. However, for $x_v D^u(x_v, \gamma^3, v)$ the situation is distinctly different, especially in the smaller-x_v region, which is weakly velocity dependent. For the velocities $0.5 \leq v \leq 0.9$ the QPDF $x_v D^u(x_v, \gamma^3, v)$ approaches $x f_1^u(x)$ in the region $x_v \lesssim (0.2\text{–}0.3)$ rather rapidly. In fact, on the scale of the upper panel of Fig. 4, the curves for $x_v D^u(x_v, \gamma^3, v)$ and $x f_1^u(x)$ cannot be distinguished for $v \geq 0.7$; see Figs. 4(b) and 4(c). In particular, the convergence of $x_v D^u(x_v, \gamma^3, v)$ in the smaller-x_v region is significantly faster than that of $x_v D^u(x_v, \gamma^0, v)$. This observation is rather remarkable. For the d-flavor the situation is very similar.

Next we discuss the $\Gamma = \gamma^0$ vs γ^3 comparison for sea quarks. Some features are similar to the quark case, but the convergence pattern is overall distinctly different for sea quarks. Let us begin with the similarity. At the low $v = 0.5$, the $x_v D^{\bar{u}}(x_v, \gamma^0, v)$ and $x_v D^{\bar{u}}(x_v, \gamma^3, v)$ basically agree with each other for larger x_v (as in the quark case), although the onset of this regime with $x_v \gtrsim 0.4$ appears at smaller x_v compared to the quark case at the same velocity. For $x_v \lesssim 0.4$ the antiquark QPDFs differ from each other more significantly than in the quark case. The reason for this is the opposite-sign leaking phenomenon in the γ^0 case compared to the same-sign leaking in the γ^3 case. The leaking happens for quarks and antiquarks. But in the quark

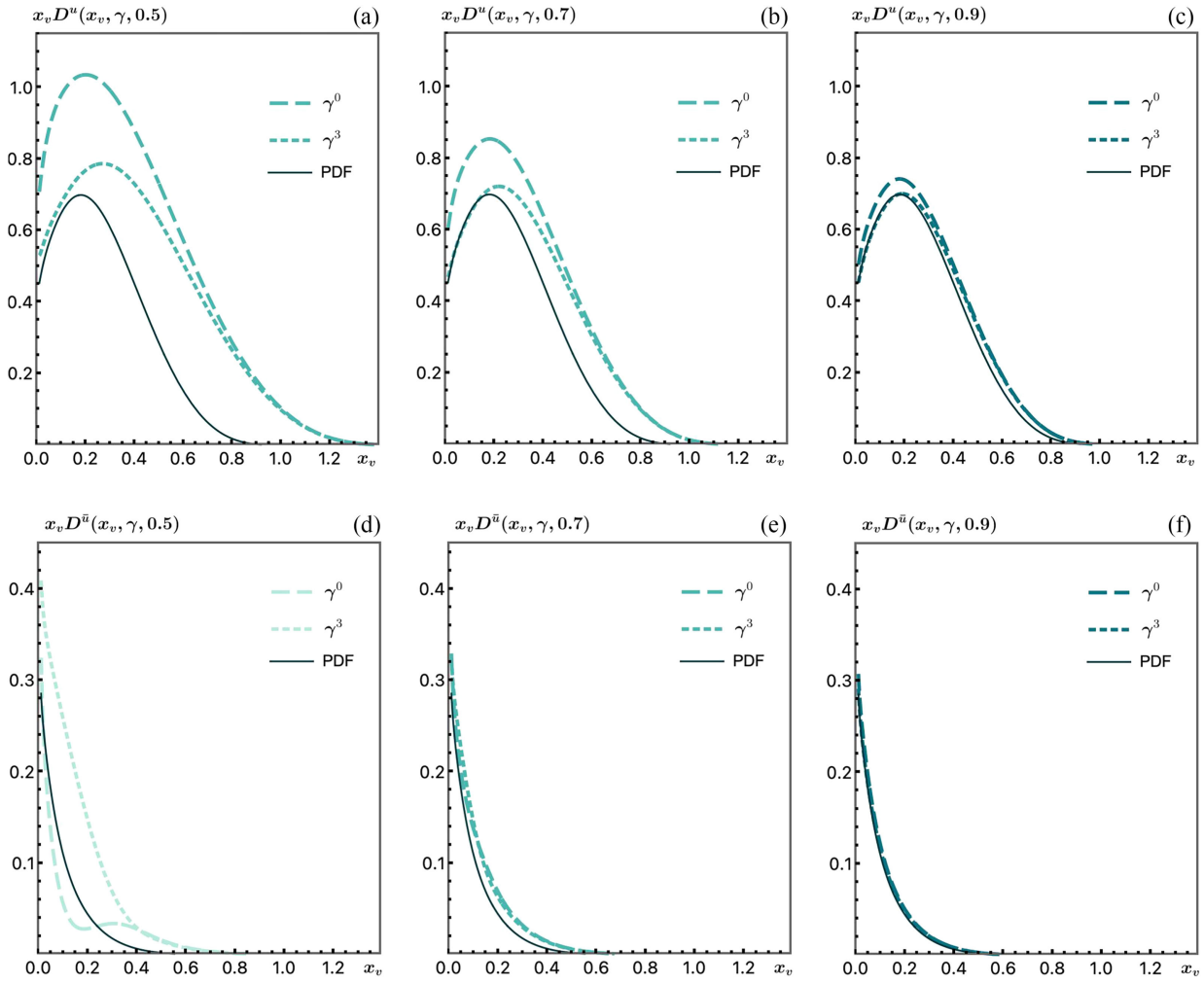


FIG. 4. The QPDFs $x_v D^a(x_v,\Gamma,v)$ for $\Gamma=\gamma^0$ and γ^3 from the CPM at different velocities with the PDFs included for comparison. Upper panel: u-quark for $v=0.5$ (a), 0.7 (b), and 0.9 (c). Lower panel: $\bar u$-antiquark for $v=0.5$ (d), 0.7 (e), and 0.9 (f). Not shown are the d-quark QPDF, which looks qualitatively similarly to the u-quark case, and other sea quark QPDFs, which exhibit similar patterns to the $\bar u$-antiquark case.

case (small $\bar q$-effects leak into the large q) the effect is much smaller than in the antiquark case (where large q-effects leak into the small $\bar q$). Recall that for still smaller velocities the leaking can even overturn the sign of $x_v D^{\bar u}(x_v,\Gamma,v)$; cf. the discussion in Sec. III C.

As v increases, the region of larger x_v extends where the γ^0 and γ^3 QPDFs are numerically close. A remarkable difference between quarks and antiquarks is that the growth of this region with increasing v proceeds much faster for antiquarks, such that $x_v D^{\bar u}(x_v,\gamma^0,v)$ and $x_v D^{\bar u}(x_v,\gamma^3,v)$ practically agree with each other (but not with the PDF) already at $v\geq 0.7$. For still higher velocities the QPDFs (of either choice for Γ) agree with the PDF already within a few percent. Thus, the convergence is overall faster for antiquark QPDFs than for quark QPDFs in the CPM. The case of the $\bar d$-flavor is very similar. For the strangeness QPDF, however, the situation is somewhat different because here, the leaking effects discriminate far less between the γ^0 and γ^3 cases, and there are no sign turnovers or wiggles at lower velocities; cf. the discussion in footnote 1.

C. CPM results in the small-x_v region

In the CPM, no restrictions arise on the x_v-range where QPDFs can be computed, unlike in other models [56] or lattice QCD; see Sec. IV E. We can therefore apply the model, for instance, to the regime of asymptotically small x_v. In Fig. 5 we show representatively the results for $D^u(x,\Gamma,v)$. Other flavors, including antiquarks, look very similar in the small-x_v region. Also, $f_1^u(x)$ is shown in Fig. 5. The pertinent asymptotics from, respectively, Eqs. (64), (66), (67) are included for comparison. In the small-x_v region, $D^u(x,\gamma^0,v)$ is larger than $D^u(x,\gamma^3,v)$ for velocities $v\gtrsim 0.5$. For lower velocities it is vice versa.

The asymptotics of $D^u(x,\gamma^0,v)$ set in at low $x_v\lesssim 10^{-3}$, that of the PDF at $x\lesssim 3\times 10^{-3}$, while for $D^u(x,\gamma^3,v)$ this happens at $x_v\lesssim 10^{-2}$. The curves for $D^u(x,\gamma^0,v)$ and

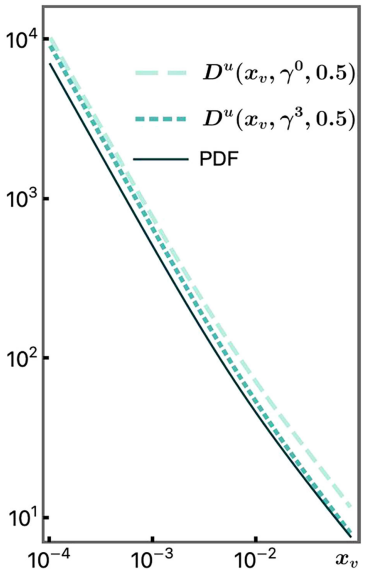


FIG. 5. $D^u(x_v, \Gamma, v)$ and $f_1^q(x)$ at $v = 0.5$ in the small-x_v region. The asymptotics in Eqs. (64)–(67) set in between $10^{-3} < x_v < 10^{-2}$ depending on the function; see text.

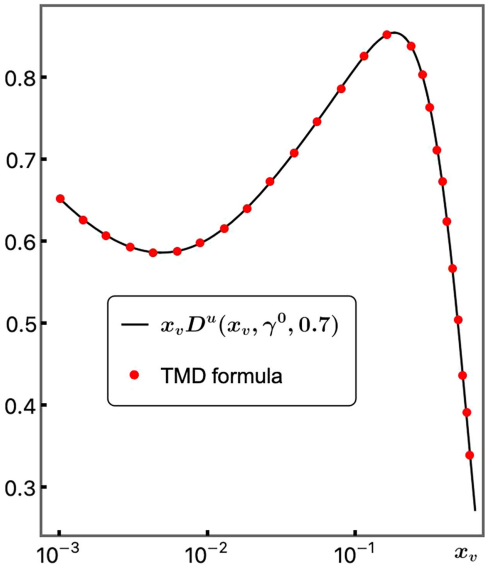


FIG. 6. $x_v D^u(x_v, \gamma^0, v)$ at $v = 0.7$ in the CPM computed directly (solid line) and via Eq. (13) (discrete points).

$D^u(x, \gamma^3, v)$ at $v = 0.5$ are closer to each other than to the PDF. The trend that $D^u(x, \gamma^3, v)$ converges faster than $D^u(x, \gamma^0, v)$ toward the PDF in the region $10^{-2} < x_v \lesssim 0.2$ observed in Fig. 4(a) (and clearly visible also in Fig. 5 for $x_v > 10^{-2}$) does not continue into the region of very small x_v. The results for the $\bar{u}$ QPDFs have exactly the same asymptotics, as otherwise the flavor number sum rule would diverge, but the asymptotics set in significantly earlier due to the absence of a valence-x_v region. For d and $\bar{d}$ the results are very similar with somewhat different numerical values for the constants A and B in Eqs. (64), (66), (67). The s and $\bar{s}$ results are analogous to the other sea quark results.

D. Test of Radyushkin formula in Eq. (13)

The relation (13) provides an important cross-check for the numerics and serves as a theoretical consistency test of the model. The model expression for the unpolarized quark TMD is given by [69]

$$f_1^q(x, \vec{k}_\perp^2) = xM^2 \Theta(x(1-x)M^2 - \vec{k}_\perp^2) \mathcal{G}^q\left(\frac{xM^2}{2} + \frac{\vec{k}_\perp^2}{2x}\right), \quad (72)$$

where the argument of $\mathcal{G}^q$ is $P \cdot k = Mk^0$ with $k^0 = \frac{xM}{2}(1 + \frac{\vec{k}_\perp^2}{x^2M^2})$.

Computing a QPDF via the Radyushkin relation is numerically more involved, since for every x_v-value one needs to determine the TMD at all values of x and $\vec{k}_\perp^2$ and then carry out integrations over dx and $d^2k_\perp$. Even in simple models, this takes up significantly more computing time than the direct calculation. We therefore content ourselves with computing the QPDF at only selected x_v, shown as bullets in Fig. 6. The Radyushkin formula is valid in the CPM within numerical accuracy.

Note that in Sec. II G we have analytically proven that this relation holds in any quark model including the CPM.

E. Comparison to lattice QCD results

Finally, it is instructive to present a comparison to a lattice QCD calculation. In Fig. 7(a) we show the model result for the unpolarized isovector QPDF $(D^u - D^d)(x_v, \gamma^0, v)$ at a scale of $\mu^2 = 4$ GeV^2 in comparison to the lattice QCD study [24] at the largest available value of nucleon momentum in [24], $P_z = 1.38$ GeV, corresponding to a nucleon velocity of $v = 0.827c$. This lattice calculation was performed on a $48^3 \times 96$ lattice with a lattice spacing $a = 0.094$ fm, a lattice size of $L = 4.5$ fm, and a practically physical pion mass of 130 MeV.

Our simple model cannot be expected to agree exactly with lattice QCD. However, the model QPDFs converge by default into the physical PDFs, and the lattice QCD results are ultimately expected to do the same. Our covariant model correctly describes the relativistic "kinematics," but it misses the "dynamics" owing to the on-shell assumption. It is therefore instructive to investigate the difference between the lattice and model results in the hope to learn something about the size of off-shellness effects. We do this in Fig. 7(b), where we plot

$$D^{u-d}_{\text{diff}}(x_v, \gamma^0, v) = (D^u - D^d)(x_v, \gamma^0, v)|_{\text{lattice}} - (D^u - D^d)(x_v, \gamma^0, v)|_{\text{CPM}} \quad (73)$$

with an uncertainty band due to the lattice data [24]. The light-shaded region in the interval $|x_v| < 0.3$ indicates the region where the lattice calculation is likely not reliable,

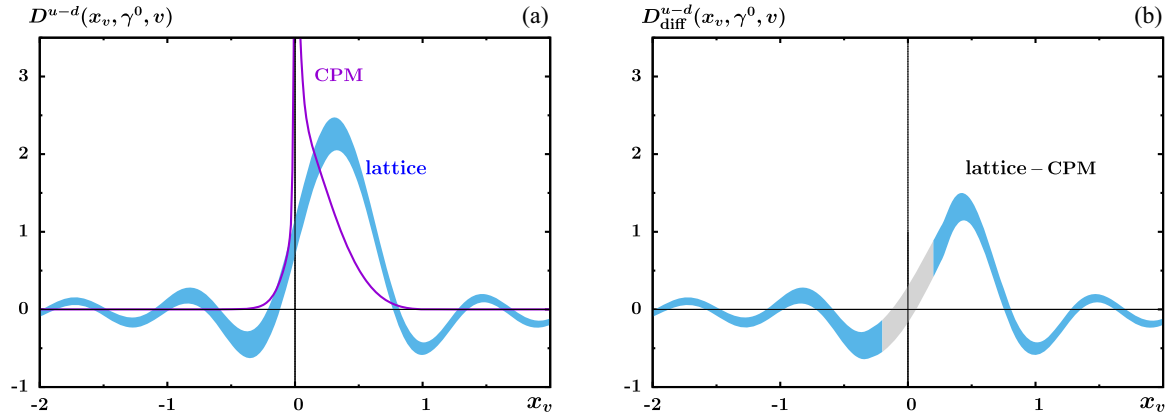


FIG. 7. (a) Unpolarized isovector QPDF $(D^u - D^d)(x_v, \gamma^0, v)$ at a scale of $\mu^2 = 4$ GeV^2 as function of x_v for $P_z = 1.38$ GeV, which corresponds $v = 0.827c$ from the lattice QCD study of Ref. [24] in comparison to the CPM results obtained in this work. (b) Difference of lattice result minus model result. The light-shaded region $|x| < 0.3$ is filled in to guide the eye; see text.

as explained below, and we removed this part, interpolating with cubic splines to guide the eye. With this reservation in mind, Fig. 7(b) seems to suggest that we may see a superposition of two effects, one being undoubtedly due to the model assumption of free partons and another possibly due to systematic effects in [24]. Despite great efforts to control such effects, lattice calculations of QPDFs are still at a pioneering stage, and the presence of uncontrolled systematic uncertainties cannot be excluded. The truncation of the Fourier transform is among the most challenging systematic effects [24], as discussed below.

The QPDF was computed in [24] by evaluating the matrix element $h^q(\nu, \gamma^0, P_z) = \frac{1}{2}\langle N_v|\bar{\Psi}^q(0)\mathcal{W}\gamma^0\Psi^q(z)|N_v\rangle$ for $z^\mu = (0, 0, 0, z^3)$ with $\nu = P^3 z^3$, which yields the QPDF via

$$D^q(x_v, \Gamma, v) = \int \frac{d\nu}{2\pi} e^{-i\nu x_v} h^q(\nu, \Gamma, P_z). \tag{74}$$

This corresponds to the quark model expression in Eq. (4) except for the appearance of the Wilson line $\mathcal{W}$. More precisely, in lattice calculations the Fourier transform is evaluated as a discrete series rather than a continuous integral. More importantly, due to the finite lattice size, the integration (or discrete summation) goes over a finite interval $-\nu_{\max} < \nu < \nu_{\max}$, with $\nu_{\max} = P_z z_{\max} = 6.5$ for $P_z = 10\frac{\pi}{L} = 1.38$ GeV and $z_{\max} = 10a$ in Ref. [24]. Since large $|\nu|$ are correlated with small $|x_v|$, the truncation at a finite $\nu_{\max}$ implies limitations to reach the small-x_v region of QPDFs on a finite lattice.[2] Two methods were used in [24] to evaluate the Fourier transform, the "standard" and "derivative" method of Ref. [17]. The QPDFs obtained with the two methods agree for $|x_v| \gtrsim 0.3$, see Fig. 30 in [24], which we used for our rough estimate of the "less reliable region," the light-shaded $|x_v|$ region in our Fig. 7(b). The result from [24] shown in our Fig. 7(b) was obtained using the standard method of Ref. [17].

The oscillatory behavior in Fig. 7(b) might be related to truncating the Fourier transform. Other methods to address this issue can be pursued, such as the Backus-Gilbert method or neural-network based methods; see [112] and references therein for the latest developments. Further dedicated studies and inclusion of higher P_z values may be needed to shed light on whether the oscillatory behavior in Fig. 7(b) is due to QCD off-shellness effects or whether also systematic Fourier transform truncation effects may contribute. The unambiguous determination of QCD off-shellness effects would provide valuable guidance for how to relax the on-shell condition in the CPM and potentially obtain a more realistic model.

V. CONCLUSIONS

We presented a study of QPDFs in quark models, defined as models without explicit gauge degrees of freedom. We assumed that the models (i) are Lorentz invariant, and (ii) the model expressions for the $A_i(P \cdot k, k^2)$ amplitudes describing the quark correlator are either finite or made finite by means of appropriate regularization or renormalization such that Lorentz invariance is preserved. Otherwise we made no assumptions whatsoever about the model dynamics. We have shown that in all such models the unpolarized QPDFs are consistently described, yield PDFs when the nucleon velocity $v \to 1$ is taken, satisfy quark flavor and momentum sum rules (if the PDFs do so in a given model), and obey the Radyushkin relation. One interesting observation is that the QPDFs in such models are elegantly and efficiently described using the nucleon velocity v rather than the nucleon momentum P_z as a

[2]This is independent of the limitation when determining PDFs from QPDFs in the limit $v \to 1$ or $P_z \to \infty$ in a matching procedure in which power corrections of the type $M^2/(x^2(1-x)P_z^2)$ emerge, which are particularly large for $x \to 0$ and $x \to 1$ [41–46], see also [111].

variable. Another interesting observation is that the QPDF with $\Gamma = \gamma^3$ contains fewer explicit power corrections than that with $\Gamma = \gamma^0$.

We have then chosen the covariant parton model as an illustration, which takes PDFs (from parametrizations) as input and allows one to compute QPDFs of quarks and antiquarks under the assumption that they are noninteracting partons, i.e., in a Wandzura-Wilczek-type approximation. Benefiting from the simplicity and lucidity of this model, we have made a number of interesting observations. For instance, while the quark and antiquark effects are clearly separated in PDFs, they contaminate each other in the case of QPDFs. We presented numerical results for the QPDFs of u, d, $\bar{u}$, $\bar{d}$, s, $\bar{s}$ flavors and investigated their convergence. In the region of larger $x_v \gtrsim 0.3$, the two choices $\Gamma = \gamma^0$ or $\Gamma = \gamma^3$ are very similar. In the region $x_v \lesssim 0.3$, the QPDF with $\Gamma = \gamma^3$ converges toward the PDF significantly faster. We also studied the small-x_v behavior, which can be done analytically in this model but is out of reach in lattice QCD. As an interesting by-product, we have shown that the energy-momentum tensor form factor $\bar{c}^q(t)$ satisfies $\bar{c}^q(0) = -\frac{1}{4}A^q(0)$ in the CPM, and hence, also in the Wandzura-Wilczek approximation. The CPM results entail the complete target-mass corrections.

We also presented a comparison to a lattice QCD calculation. Since the model results for QPDFs converge to the correct PDFs as do the lattice results, we investigated the difference in lattice and model results in the hope to obtain insight on the size of off-shellness effects in QPDFs. At the present stage, it is unclear whether the observed difference is due to off-shellness effects or might include also systematic effects, which are not yet under full control in pioneering lattice studies like, e.g., effects due to the truncation of the Fourier transform. Insights on off-shellness effects would be very interesting, as they could guide novel developments to relax the on-shell restriction in the CPM and construct more realistic models.

The advantage of the CPM model framework is its fully field-theoretical description of the unintegrated quark correlator, which allows one to describe QPDFs and TMDs in terms of PDFs, which serve as input for this model. The next steps will include applications to polarized QPDFs and subleading twist. The results might give helpful insights for the extrapolation of QPDFs in lattice QCD.

ACKNOWLEDGMENTS

We thank Shohini Bhattacharya, Krzysztof Cichy, and Martha Constantinou for valuable discussions and making the lattice results of [24] available. This work was supported by the NSF, Award No. 2412625, and the DOE Quark-Gluon Tomography Topical Collaboration with Award No. DE-SC0023646.

DATA AVAILABILITY

There are no publicly available research data or software supporting this manuscript. Requests for further information or data should be sent to the authors.

APPENDIX A: CONVENTIONS OF QPDFS IN THE LITERATURE

Different conventions have been used in the literature. For clarity and to reduce confusion, we provide some comments and comparisons here. In the velocity formulation of QPDFs, the different conventions can be simply stated as

$$D^q(x_v,\Gamma,v)\Big|_{\text{this work}} = D^q(x_v,\Gamma,v)\Big|_{\text{Ref. [3]}} = \frac{1}{v}D^q(x_v,\Gamma,v)\Big|_{\text{Ref. [5,56]}}. \tag{A1}$$

In Refs. [34,35] only the QPDF for the case $\Gamma = \gamma^0$ was discussed. The connection to our notation is as follows:

$$D^q(x_v,\gamma^0,v)\Big|_{\text{this work}} = \frac{1}{v}D^q(x_v,\gamma^0,v)\Big|_{\text{Ref. [34,35]}}. \tag{A2}$$

One convenient way to quickly verify the underlying conventions is to compare the sum rules $\int dx_v^k D^q(x_v,\Gamma,v)$ for $k = 0,\ 1$ in Eqs. (9), (11), (10), (12) in our work vs the sum rules in Eqs. (21), (25) of [56] or Eqs. (2.25), (2.28) of [34], which differ by factors of v according to Eqs. (A1), (A2).

As a consequence of different conventions, the formula (13) relating QPDFs and TMDs is formulated in our convention with the prefactor P_0, while in [34] it was originally derived with the prefactor of $P_z = vP_0$.

APPENDIX B: DIRAC FORM FACTOR $F_1^q(0)$

In the appendixes, the four-momenta P^μ and k^μ are understood in a general reference frame unless we explicitly specify otherwise. In this appendix we derive the expression for the Dirac form factor in the forward limit.

The contribution of the quark flavor q to the electromagnetic current operator is given by $J_q^\mu(y) = \bar{\Psi}_q(y)\gamma^\mu\Psi_q(y)$. The nucleon matrix elements of this operator are described in terms of the electromagnetic form factors as follows:

$$\langle N'|J_q^\mu(y)|N\rangle = \bar{u}_{N'}\left[\gamma^\mu F_1^q(t) + \frac{i\sigma_{\mu\nu}\Delta_\nu}{2M}F_2^q(t)\right]u_N e^{i\Delta\cdot y}, \tag{B1}$$

where $\Delta^\mu = P'^\mu - P^\mu$ and $t = \Delta^2$, and $|N\rangle = |P,S\rangle$ denotes the nucleon state. The nucleon spinors $u_N = u(P,S)$ are normalized as $\bar{u}_N u_N = 2M$. Using the identity $\bar{u}_N\gamma^\mu u_N = 2P^\mu$ we obtain in the forward limit the expression

$$\langle N|J_q^\mu(y)|N\rangle = 2P^\mu F_1^q(0), \tag{B2}$$

which we wish to evaluate in quark models in terms of the $A_i^q(P\cdot k, k^2)$ amplitudes. Notice that translation invariance allows us to arbitrarily shift the position y of the operator, which introduces an overall phase in the off-forward case (B1) and literally has no effect in the forward case (B2). It is convenient to choose $y = 0$.

In order to derive the expressions for $\langle N|J_q^\mu(y)|N\rangle$ in quark models in terms of amplitudes A_i^q, we proceed as follows. Based on Eq. (14), we obtain

$$\int \frac{d^4z}{(2\pi)^4} e^{ik\cdot z}\langle N|\bar\Psi^q(0)\gamma^\mu\Psi^q(z)|N\rangle = \mathrm{tr}[\Phi^q(k,P,S)\gamma^\mu]. \tag{B3}$$

The Fourier transform of this expression yields

$$\langle N|\bar\Psi^q(0)\gamma^\mu\Psi^q(z)|N\rangle = \int d^4k\, e^{-ik\cdot z}\,\mathrm{tr}[\Phi^q(k,P,S)\gamma^\mu]. \tag{B4}$$

Being interested in the local operator $J_q^\mu(0) = \bar\Psi_q(0)\gamma^\mu\Psi_q(0)$, we set $z = 0$ in Eq. (B4) and obtain

$$\begin{aligned}\langle N|J_q^\mu(0)|N\rangle &= 2P^\mu\, F_1^q(0) = \int d^4k\,\mathrm{tr}[\Phi^q(k,P,S)\gamma^\mu]\\ &= 4\int d^4k(P^\mu A_2^q + k^\mu A_3^q),\end{aligned} \tag{B5}$$

where in the last step we made use of Eq. (18). We now choose to evaluate Eq. (B5) in the nucleon rest frame specified by Eq. (21). This yields

$$F_1^q(0) = 2\int d^4k\left(A_2^q + \frac{k^0}{M}A_3^q\right). \tag{B6}$$

Notice that the expression in Eq. (B5) contains under the d^4k integral terms proportional to $k^iA_3^q$, which are odd functions and drop out after integration. Only the expectation value of the $J_q^0(0)$ component yields a nonzero result, which corresponds to the electric charge. It is customary to define

$$F_1^q(0) = N^q \tag{B7}$$

with $N^u = 2$ and $N^d = 1$ for proton (vice versa for neutron). The convention is that the nucleon Dirac form factor is given by $F_1(t) = \sum_q e_q F_1^q(t)$, where $e_u = \frac{2}{3}$, etc. are the quark fractional charges. At $t = 0$ one recovers the electric charge of the particle in units of the elementary unit of charge, i.e., the value $F_1(0) = 1$ for proton (zero for neutron).

We notice that that the expression for $F_1^q(0) = N^q$ was encountered in the sum rules in Eqs. (26)–(28), which completes the proof of the quark flavor sum rules in Eqs. (7), (9), (11).

APPENDIX C: ENERGY-MOMENTUM TENSOR FORM FACTORS $A^q(0)$ AND $\bar c^q(0)$

With the notation introduced in the previous section and the definition $\bar P^\mu = \frac{1}{2}(P'^\mu + P^\mu)$, the nucleon form factors of the quark contribution to the energy-momentum tensor (for a review see, e.g., [81,82]) can be defined as

$$\begin{aligned}\langle N'|\hat T_q^{\mu\nu}(0)|N\rangle = \bar u_{N'}\Bigg[&A^q(t)\frac{\bar P_\mu\bar P_\nu}{M}\\ &+ J^q(t)\frac{i(\bar P_\mu\sigma_{\nu\rho}+\bar P_\nu\sigma_{\mu\rho})\Delta^\rho}{2M}\\ &+ D^q(t)\frac{\Delta_\mu\Delta_\nu - g_{\mu\nu}\Delta^2}{4M} + \bar c^q(t)Mg^{\mu\nu}\Bigg]u_N.\end{aligned} \tag{C1}$$

We are interested in the forward limit of this expression, which is given by

$$\langle N|\hat T_q^{\mu\nu}(0)|N\rangle = 2P_\mu P_\nu A^q(0) + 2M^2 g^{\mu\nu}\bar c^q(0). \tag{C2}$$

Notice that the zero on the left-hand side is the position of the operator $T_q^{\mu\nu}(y)$, which, based on translational invariance, can be conveniently chosen $y = 0$, while the zero on the right-hand side is the momentum transfer square $t = 0$.

While the total energy-momentum tensor operator depends on the details and degrees of freedom in a model, the expression for the quark part of this operator is given in all quark models by

$$T_q^{\mu\nu}(0) = \frac{1}{4}\bar\Psi_q(0)(-i\overleftarrow\partial^\mu\gamma^\nu - i\overleftarrow\partial^\nu\gamma^\mu + i\vec\partial^\mu\gamma^\nu + i\vec\partial^\nu\gamma^\mu)\Psi_q(0), \tag{C3}$$

where the arrows indicate whether $\bar\Psi_q(0)$ or $\Psi_q(0)$ are to be differentiated. In order to evaluate the matrix elements of this operator we carry out the following steps:

$$\begin{aligned}&\int \frac{\mathrm{d}^4z}{(2\pi)^4}\mathrm{e}^{ik\cdot z}\langle N|\bar\Psi^q(0)\gamma^\mu(i\vec\partial^\nu\Psi^q(z))|N\rangle\\ &= \mathrm{tr}[\Phi^q(k,P,S)\gamma^\mu k^\nu],\end{aligned} \tag{C4}$$

$$\begin{aligned}&\int \frac{\mathrm{d}^4z}{(2\pi)^4}\mathrm{e}^{-ik\cdot z}\langle N|(-\bar\Psi^q(z)i\overleftarrow\partial^\nu)\gamma^\mu\Psi^q(0)|N\rangle\\ &= \mathrm{tr}[\Phi^q(k,P,S)\gamma^\mu k^\nu].\end{aligned} \tag{C5}$$

In Eq. (C4) on the left-hand side we perform an integration by parts and use the definition of the correlator (14). In Eq. (C5) we perform an integration by parts, use translation invariance to shift the positions of the operator as

$\langle N|\bar{\Psi}^q(z)\gamma^\mu\Psi^q(0)|N\rangle = \langle N|\bar{\Psi}^q(0)\gamma^\mu\Psi^q(-z)|N\rangle$, and substitute $z^\mu \to (-z^\mu)$ before using the correlator definition. Inverting the Fourier transforms in Eqs. (C4), (C5), repeating the steps with exchanged indices $\mu \leftrightarrow \nu$, adding up all pieces, and taking finally the limit $z^\mu \to 0$ to recover the local operator $T_q^{\mu\nu}(0)$, we obtain from Eq. (C2)

$$\begin{aligned}\langle N|\hat{T}_q^{\mu\nu}(0)|N\rangle &= 2P_\mu P_\nu A^q(0) + 2M^2 g^{\mu\nu}\bar{c}^q(0)\\ &= 4\int d^4k\left(\frac{P^\mu k^\nu + P^\nu k^\mu}{2}A_2^q + k^\mu k^\nu A_3^q\right).\end{aligned} \tag{C6}$$

In order to derive the expressions for the form factors $A^q(0)$ and $\bar{c}^q(0)$ we contract Eq. (C6) with, respectively, $g^{\mu\nu}$ and $P^\mu P^\nu$, which yields two equations for two unknowns:

$$\begin{aligned}A^q(0) + 4\bar{c}^q(0) &= 2\int d^4k\left(\frac{P\cdot k}{M^2}A_2^q + \frac{k^2}{M^2}A_3^q\right),\\ A^q(0) + \bar{c}^q(0) &= 2\int d^4k\left(\frac{P\cdot k}{M^2}A_2^q + \frac{(P\cdot k)^2}{M^4}A_3^q\right).\end{aligned} \tag{C7}$$

Solving this simple system of linear equations yields

$$\begin{aligned}A^q(0) &= \frac{2}{3}\int d^4k\left(\frac{2(P\cdot k)^2}{M^4} + \frac{k^2}{M^2}\right)A_3^q + 2\int d^4k\frac{P\cdot k}{M^2}A_2^q,\\ \bar{c}^q(0) &= \frac{2}{3}\int d^4k\left(-\frac{(P\cdot k)^2}{M^4} + \frac{k^2}{M^2}\right)A_3^q.\end{aligned} \tag{C8}$$

So far the expressions are manifestly Lorentz invariant. Now we choose to evaluate them in the nucleon rest frame (21) [or in the frame (22), which yields the same result]. We obtain

$$\begin{aligned}A^q(0) &= \int d^4k\left(2\frac{k_0^2}{M^2} + \frac{2}{3}\frac{\vec{k}^2}{M^2}\right)A_3^q + 2\int d^4k\frac{k^0}{M}A_2^q,\\ \bar{c}^q(0) &= \int d^4k\left(-\frac{2}{3}\frac{\vec{k}^2}{M^2}\right)A_3^q.\end{aligned} \tag{C9}$$

The above expression for $A^q(0)$ was encountered in the momentum sum rules in Eqs. (29)–(31). We also recognize that the expression for $\bar{c}^q(0)$ appears in the momentum sum rule for the QPDF $D^q(x_v, \gamma^3, v)$ in Eq. (31). This completes the proof of the momentum sum rules Eqs. (7), (9), (11).

[1] J. C. Collins and D. E. Soper, Nucl. Phys. **B194**, 445 (1982).
[2] J. C. Collins, D. E. Soper, and G. F. Sterman, Adv. Ser. Dir. High Energy Phys. **5**, 1 (1989).
[3] X. Ji, Phys. Rev. Lett. **110**, 262002 (2013).
[4] X. Ji, Sci. China Phys. Mech. Astron. **57**, 1407 (2014).
[5] D. Diakonov, V. Y. Petrov, P. V. Pobylitsa, M. V. Polyakov, and C. Weiss, Phys. Rev. D **56**, 4069 (1997).
[6] X. Xiong, X. Ji, J. H. Zhang, and Y. Zhao, Phys. Rev. D **90**, 014051 (2014).
[7] I. W. Stewart and Y. Zhao, Phys. Rev. D **97**, 054512 (2018).
[8] T. Izubuchi, X. Ji, L. Jin, I. W. Stewart, and Y. Zhao, Phys. Rev. D **98**, 056004 (2018).
[9] X. Ji, Y. S. Liu, Y. Liu, J. H. Zhang, and Y. Zhao, Rev. Mod. Phys. **93**, 035005 (2021).
[10] H. W. Lin, J. W. Chen, S. D. Cohen, and X. Ji, Phys. Rev. D **91**, 054510 (2015).
[11] C. Alexandrou, K. Cichy, V. Drach, E. Garcia-Ramos, K. Hadjiyiannakou, K. Jansen, F. Steffens, and C. Wiese, Phys. Rev. D **92**, 014502 (2015).
[12] J. W. Chen, S. D. Cohen, X. Ji, H. W. Lin, and J. H. Zhang, Nucl. Phys. **B911**, 246 (2016).
[13] C. Alexandrou, K. Cichy, M. Constantinou, K. Hadjiyiannakou, K. Jansen, F. Steffens, and C. Wiese, Phys. Rev. D **96**, 014513 (2017).
[14] C. Alexandrou, K. Cichy, M. Constantinou, K. Hadjiyiannakou, K. Jansen, H. Panagopoulos, and F. Steffens, Nucl. Phys. **B923**, 394 (2017).
[15] J. W. Chen, T. Ishikawa, L. Jin, H. W. Lin, Y. B. Yang, J. H. Zhang, and Y. Zhao, Phys. Rev. D **97**, 014505 (2018).
[16] J. Green, K. Jansen, and F. Steffens, Phys. Rev. Lett. **121**, 022004 (2018).
[17] H. W. Lin *et al.* (LP3 Collaboration), Phys. Rev. D **98**, 054504 (2018).
[18] C. Alexandrou, K. Cichy, M. Constantinou, K. Jansen, A. Scapellato, and F. Steffens, Phys. Rev. Lett. **121**, 112001 (2018).
[19] J. H. Zhang, J. W. Chen, L. Jin, H. W. Lin, A. Schäfer, and Y. Zhao, Phys. Rev. D **100**, 034505 (2019).
[20] C. Alexandrou, K. Cichy, M. Constantinou, K. Jansen, A. Scapellato, and F. Steffens, Phys. Rev. D **98**, 091503 (2018).
[21] Y. S. Liu *et al.* (Lattice Parton Collaboration), Phys. Rev. D **101**, 034020 (2020).
[22] H. W. Lin, J.-W. Chen, X. Ji, L. Jin, R. Li, Y.-S. Liu, Y.-B. Yang, J.-H. Zhang, and Y. Zhao, Phys. Rev. Lett. **121**, 242003 (2018).
[23] Z. Y. Fan, Y. B. Yang, A. Anthony, H. W. Lin, and K. F. Liu, Phys. Rev. Lett. **121**, 242001 (2018).
[24] C. Alexandrou, K. Cichy, M. Constantinou, K. Hadjiyiannakou, K. Jansen, A. Scapellato, and F. Steffens, Phys. Rev. D **99**, 114504 (2019).
[25] T. Izubuchi, L. Jin, C. Kallidonis, N. Karthik, S. Mukherjee, P. Petreczky, C. Shugert, and S. Syritsyn, Phys. Rev. D **100**, 034516 (2019).

[26] S. Bhattacharya, K. Cichy, M. Constantinou, A. Metz, A. Scapellato, and F. Steffens, Phys. Rev. D **102**, 111501 (2020).
[27] S. Bhattacharya, K. Cichy, M. Constantinou, A. Metz, A. Scapellato, and F. Steffens, Phys. Rev. D **104**, 114510 (2021).
[28] X. Gao, A. D. Hanlon, S. Mukherjee, P. Petreczky, P. Scior, S. Syritsyn, and Y. Zhao, Phys. Rev. Lett. **128**, 142003 (2022).
[29] J. Delmar, C. Alexandrou, K. Cichy, M. Constantinou, and K. Hadjiyiannakou, Phys. Rev. D **108**, 094515 (2023).
[30] V. Braun, P. Górnicki, and L. Mankiewicz, Phys. Rev. D **51**, 6036 (1995).
[31] W. Detmold and C. J. D. Lin, Phys. Rev. D **73**, 014501 (2006).
[32] V. Braun and D. Mueller, Eur. Phys. J. C **55**, 349 (2008).
[33] Y. Q. Ma and J. W. Qiu, Phys. Rev. D **98**, 074021 (2018).
[34] A. V. Radyushkin, Phys. Lett. B **767**, 314 (2017).
[35] A. V. Radyushkin, Phys. Rev. D **96**, 034025 (2017).
[36] A. V. Radyushkin, Phys. Lett. B **781**, 433 (2018).
[37] A. J. Chambers, R. Horsley, Y. Nakamura, H. Perlt, P. E. L. Rakow, G. Schierholz, A. Schiller, K. Somfleth, R. D. Young, and J. M. Zanotti, Phys. Rev. Lett. **118**, 242001 (2017).
[38] M. T. Hansen, H. B. Meyer, and D. Robaina, Phys. Rev. D **96**, 094513 (2017).
[39] K. Orginos, A. Radyushkin, J. Karpie, and S. Zafeiropoulos, Phys. Rev. D **96**, 094503 (2017).
[40] Y. Q. Ma and J. W. Qiu, Phys. Rev. Lett. **120**, 022003 (2018).
[41] H. W. Lin *et al.*, Prog. Part. Nucl. Phys. **100**, 107 (2018).
[42] C. Monahan, Proc. Sci. LATTICE 2018 (**2018**) 018 [arXiv:1811.00678].
[43] K. Cichy and M. Constantinou, Adv. High Energy Phys. **2019**, 3036904 (2019).
[44] Y. Zhao, Int. J. Mod. Phys. A **33**, 1830033 (2019).
[45] M. Constantinou, Eur. Phys. J. A **57**, 77 (2021).
[46] M. Constantinou, L. Del Debbio, X. Ji, H. W. Lin, K. F. Liu, C. Monahan, K. Orginos, P. Petreczky, J. W. Qiu, D. Richards *et al.*, arXiv:2202.07193.
[47] L. Gamberg, Z. B. Kang, I. Vitev, and H. Xing, Phys. Lett. B **743**, 112 (2015).
[48] A. Bacchetta, M. Radici, B. Pasquini, and X. Xiong, Phys. Rev. D **95**, 014036 (2017).
[49] W. Broniowski and E. Ruiz Arriola, Phys. Lett. B **773**, 385 (2017).
[50] T. J. Hobbs, Phys. Rev. D **97**, 054028 (2018).
[51] W. Broniowski and E. Ruiz Arriola, Phys. Rev. D **97**, 034031 (2018).
[52] S. S. Xu, L. Chang, C. D. Roberts, and H. S. Zong, Phys. Rev. D **97**, 094014 (2018).
[53] S. Bhattacharya, C. Cocuzza, and A. Metz, Phys. Lett. B **788**, 453 (2019).
[54] V. M. Braun, A. Vladimirov, and J. H. Zhang, Phys. Rev. D **99**, 014013 (2019).
[55] S. Bhattacharya, C. Cocuzza, and A. Metz, Phys. Rev. D **102**, 054021 (2020).
[56] H. D. Son, A. Tandogan, and M. V. Polyakov, Phys. Lett. B **808**, 135665 (2020).
[57] Z. L. Ma, J. Q. Zhu, and Z. Lu, Phys. Rev. D **101**, 114005 (2020).
[58] A. Kock, Y. Liu, and I. Zahed, Phys. Rev. D **102**, 014039 (2020).
[59] H. D. Son, Phys. Lett. B **838**, 137741 (2023).
[60] V. Shastry, W. Broniowski, and E. Ruiz Arriola, Phys. Rev. D **106**, 114035 (2022).
[61] C. Tan and Z. Lu, Phys. Rev. D **106**, 094003 (2022).
[62] R. P. Feynman, Phys. Rev. Lett. **23**, 1415 (1969).
[63] R. P. Feynman, *Photon-Hadron Interactions* (W.A.Benjamin, INC., Reading, 1972).
[64] P. Zavada, Phys. Rev. D **55**, 4290 (1997).
[65] P. Zavada, Phys. Rev. D **65**, 054040 (2002).
[66] P. Zavada, Phys. Rev. D **67**, 014019 (2003).
[67] A. V. Efremov, O. V. Teryaev, and P. Zavada, Phys. Rev. D **70**, 054018 (2004).
[68] P. Zavada, Eur. Phys. J. C **52**, 121 (2007).
[69] A. V. Efremov, P. Schweitzer, O. V. Teryaev, and P. Zavada, Phys. Rev. D **80**, 014021 (2009).
[70] U. D'Alesio, E. Leader, and F. Murgia, Phys. Rev. D **81**, 036010 (2010).
[71] P. Zavada, Phys. Rev. D **83**, 014022 (2011).
[72] A. V. Efremov, P. Schweitzer, O. V. Teryaev, and P. Zavada, arXiv:0912.3380.
[73] A. V. Efremov, P. Schweitzer, O. V. Teryaev, and P. Zavada, Phys. Rev. D **83**, 054025 (2011).
[74] P. Zavada, Phys. Rev. D **85**, 037501 (2012).
[75] P. Zavada, Phys. Rev. D **89**, 014012 (2014).
[76] P. Zavada, Phys. Lett. B **751**, 525 (2015).
[77] S. Bastami, A. V. Efremov, P. Schweitzer, O. V. Teryaev, and P. Zavada, Phys. Rev. D **103**, 014024 (2021).
[78] F. Aslan, S. Bastami, and P. Schweitzer, Nucl. Phys. **B984**, 115947 (2022).
[79] F. Aslan, S. Bastami, A. Mahabir, A. Tandogan, and P. Schweitzer, Phys. Rev. D **106**, 096010 (2022).
[80] J. Blümlein and N. Kochelev, Phys. Lett. B **381**, 296 (1996).
[81] M. V. Polyakov and P. Schweitzer, Int. J. Mod. Phys. A **33**, 1830025 (2018).
[82] V. D. Burkert, L. Elouadrhiri, F. X. Girod, C. Lorcé, P. Schweitzer, and P. E. Shanahan, Rev. Mod. Phys. **95**, 041002 (2023).
[83] P. J. Mulders and R. D. Tangerman, Nucl. Phys. **B461**, 197 (1996); **B484**, 538(E) (1997).
[84] K. Goeke, A. Metz, and M. Schlegel, Phys. Lett. B **618**, 90 (2005).
[85] A. Metz, P. Schweitzer, and T. Teckentrup, Phys. Lett. B **680**, 141 (2009).
[86] T. Teckentrup, A. Metz, and P. Schweitzer, Mod. Phys. Lett. A **24**, 2950 (2009).
[87] D. Boer and P. J. Mulders, Phys. Rev. D **57**, 5780 (1998).
[88] M. Constantinou and H. Panagopoulos, Phys. Rev. D **96**, 054506 (2017).
[89] J. W. Chen, L. Jin, H. W. Lin, Y. S. Liu, Y. B. Yang, J. H. Zhang, and Y. Zhao, arXiv:1803.04393.
[90] M. Constantinou, A. Courtoy, M. A. Ebert, M. Engelhardt, T. Giani, T. Hobbs, T. J. Hou, A. Kusina, K. Kutak, J. Liang *et al.*, Prog. Part. Nucl. Phys. **121**, 103908 (2021).
[91] C. Lorcé, B. Pasquini, and P. Schweitzer, J. High Energy Phys. 01 (2015) 103.

[92] S. J. Brodsky, H. C. Pauli, and S. S. Pinsky, Phys. Rep. **301**, 299 (1998).
[93] T. J. Hou, K. Xie, J. Gao, S. Dulat, M. Guzzi, T. J. Hobbs, J. Huston, P. Nadolsky, J. Pumplin, C. Schmidt *et al.*, arXiv:1908.11394.
[94] R. Boussarie, M. Burkardt, M. Constantinou, W. Detmold, M. Ebert, M. Engelhardt, S. Fleming, L. Gamberg, X. Ji, Z. B. Kang *et al.*, arXiv:2304.03302.
[95] S. Bastami, H. Avakian, A. V. Efremov, A. Kotzinian, B. U. Musch, B. Parsamyan, A. Prokudin, M. Schlegel, G. Schnell, P. Schweitzer *et al.*, J. High Energy Phys. 06 (2019) 007.
[96] X. D. Ji, W. Melnitchouk, and X. Song, Phys. Rev. D **56**, 5511 (1997).
[97] M. J. Neubelt, A. Sampino, J. Hudson, K. Tezgin, and P. Schweitzer, Phys. Rev. D **101**, 034013 (2020).
[98] H. Avakian, A. V. Efremov, P. Schweitzer, and F. Yuan, Phys. Rev. D **81**, 074035 (2010).
[99] K. Goeke, J. Grabis, J. Ossmann, M. V. Polyakov, P. Schweitzer, A. Silva, and D. Urbano, Phys. Rev. D **75**, 094021 (2007).
[100] H. Y. Won, H. C. Kim, and J. Y. Kim, Phys. Lett. B **850**, 138489 (2024).
[101] M. V. Polyakov and H. D. Son, J. High Energy Phys. 09 (2018) 156.
[102] C. Lorcé, Eur. Phys. J. C **78**, 120 (2018).
[103] K. F. Liu, Phys. Rev. D **104**, 076010 (2021).
[104] A. Accardi, A. Bacchetta, W. Melnitchouk, and M. Schlegel, J. High Energy Phys. 11 (2009) 093.
[105] Y. Hatta, A. Rajan, and K. Tanaka, J. High Energy Phys. 12 (2018) 008.
[106] X. D. Ji, Phys. Rev. Lett. **74**, 1071 (1995).
[107] A. Metz, B. Pasquini, and S. Rodini, Phys. Rev. D **102**, 114042 (2020).
[108] X. Ji, Y. Liu, and A. Schäfer, Nucl. Phys. **B971**, 115537 (2021).
[109] C. Lorcé, A. Metz, B. Pasquini, and S. Rodini, J. High Energy Phys. 11 (2021) 121.
[110] J. Collins, T. C. Rogers, and N. Sato, Phys. Rev. D **105**, 076010 (2022).
[111] S. Bhattacharya, K. Cichy, M. Constantinou, A. Metz, A. Scapellato, and F. Steffens, Phys. Rev. D **102**, 114025 (2020).
[112] M. H. Chu, K. Cichy, M. Constantinou, P. Sznajder, and J. Wagner, J. High Energy Phys. 05 (2026) 210.